

Ultrafast relaxation dynamics of excited carriers in metals: Simplifying the intertwined dependencies upon scattering strengths, phonon temperature, photon energy, and excitation level

D. M. Riffe*

Physics Department, Utah State University, Logan, UT 84322, USA

Richard B. Wilson

*Mechanical Engineering Department and Materials Science and Engineering Department,
University of California, Riverside, CA 92521, USA*

(Dated: January 31, 2024)

Using the Boltzmann transport equation (BTE), we study the evolution of nonequilibrium carrier distributions in simple (*sp*) metals, assumed to have been instantaneously excited by an ultrafast laser pulse with photon energy $h\nu$. The mathematical structure of the BTE scattering integrals reveals that $h\nu$ is a natural energy scale for describing the dynamics. Normalizing all energy quantities by $h\nu$ leads to a set of three unitless parameters— β/δ , γ , and α —that control the relaxation dynamics: β/δ is the normalized ratio of electron-phonon to electron-electron scattering strengths, γ is the normalized phonon (lattice) temperature, and α is the normalized absorbed energy density. Using this theory, we systematically investigate relaxation times for the high-energy part of the distribution (τ_H), energy transfer to the phonon subsystem (τ_E), and intracARRIER thermalization (τ_{th}). In the linear region of response (valid when α is sufficiently small), we offer heuristic descriptions of each of these relaxation times as functions of β/δ and γ . Our results as a function of excitation level α show that many ultrafast experimental investigations lie in a transition region between low excitation (where the relaxation times are independent of α) and high excitation (where the two-temperature model of carrier dynamics is valid). Approximate boundaries that separate these three regions are described by simple expressions involving the normalized parameters of our model.

I. INTRODUCTION

The carrier relaxation dynamics of an ultrafast-laser-excited metal are important to a number of current scientific endeavors, including ultrafast magnetism [1–8], hot-carrier induced photocatalysis [9–12], solar-energy conversion [13–15], interpretation of ultrafast x-ray [16–19] and electron [20–26] diffraction, and inelastic light-scattering and photoluminescence signals from plasmonic materials [12, 27–38]. As we discuss in detail here, in any given experiment there are five key parameters that govern the relaxation: the electron-phonon (*ep*) scattering strength K_{ep} , electron-electron (*ee*) scattering strength K_{ee} , phonon temperature T_p , laser photon energy $h\nu$, and absorbed energy density u_a . Indeed, in any ultrafast-laser investigation of a metal these parameters (or some subset) are typically utilized to make quantitative sense of the results.

In addition to calculations aimed at describing the results of any particular experiment, a number of theoretical studies have made progress in discerning how these five parameters contribute to general trends associated with ultrafast carrier relaxation [39–48]. In general, this work utilizes the Boltzmann transport equation (BTE)

to gain insight into the consequences of simultaneous electron-phonon and electron-electron scattering. Taken separately, the basic effects of these two scattering mechanisms are simple: electron-electron scattering evolves a nonthermal carrier distribution into a thermal one, and electron-phonon scattering mediates energy transfer from the excited carriers to vibrational degrees of freedom. Taken together, however, the two scattering mechanisms intertwine to produce nontrivial dynamics.

Several studies explore these dynamics in the low-excitation limit. The early BTE computations of Groenewald *et al.* reveal what is now a fundamental tenet of excited carrier dynamics: strong *ee* scattering enhances energy transfer to the phonons [39, 40]. This effect is due to the increase in carrier number associated with intracARRIER thermalization. Gusev and Wright analytically study the BTE to extract details of this synergism and find the energy transfer time τ_E is proportional to $(\tau_0)^{1/3}(\tau_S)^{2/3}$ (their notation), where τ_0 is a characteristic *ee* scattering time and τ_S is the time for a single carrier to lose some fixed amount of energy [41]. Gusev and Wright also investigate intracARRIER thermalization and deduce if *ep* scattering is relatively weak, then the thermalization time τ_{th} is proportional to T_p^{-2} . Wilson and Coh numerically integrate the BTE to investigate carrier dynamics as a function of the ratio of *ep* to *ee* scattering strengths in the low-excitation limit [42]. They confirm energy relaxation has a nontrivial relationship to the two scattering mechanisms. In a range of ratios that applies

* Author to whom correspondence should be addressed; electronic mail: mark.riffe@usu.edu

to many metals, they find $\tau_E \sim (\tau_0)^{1/4}(\tau_S)^{3/4}$, a result not unlike that of Gusev and Wright. They also derive a more general heuristic relationship for τ_E . In addition, Wilson and Coh show relaxation of the highest energy carriers is typically controlled by ee scattering. Kabanov and coworkers explore the mathematical structure of the BTE scattering integrals in detail, deriving approximate solutions for the BTE in various limits [43, 44]. They show (for typical metals such as Au and Ru) that by the time excited carriers can be considered thermalized those carriers have already lost a large fraction of their energy to the phonons [44]. Evidently, in at least some circumstances thermalization and energy relaxation take place on similar timescales.

A few studies look at the dependence of carrier relaxation upon excitation level. Via general consideration of an approximate ee scattering integral, Tas and Maris infer τ_{th} is proportional to u_a^{-1} [45]. Other calculations of intracARRIER thermalization focus on specific materials. The numerical studies of Al by Rethfeld *et al.* [46] and Al and Au by Mueller and Rethfeld [48] show a substantial decrease in τ_{th} as the absorbed energy density is increased, but the dependence on u_a is not as simple as that suggested by Tas and Maris. The study of Al by Rethfeld *et al.* [46] and a study of Ag by Pietanza *et al.* [47] investigate the energy decay of several laser excited distributions. Both studies show if u_a is large enough, then energy decay of the laser excited distribution is indistinguishable from that of a thermal [i.e., Fermi-Dirac (FD)] distribution. Additionally, the calculations of Rethfeld *et al.* show the timescale for carrier cooling becomes larger with increasing laser excitation [46].

To summarize, three important timescales are identified by these prior investigations. The first is the timescale τ_H for relaxation of the high-energy part of the distribution [42]. The second is the timescale τ_E for transfer of energy from the excited electrons to the phonons [39–44, 46, 47]. The third is the timescale τ_{th} for intracARRIER thermalization of the laser excited distribution [41, 43–48].

Unfortunately, a systematic understanding of the dependence of these three timescales on the five key parameters— K_{ep} , K_{ee} , T_p , u_a , and $h\nu$ —is still decidedly lacking. Partly this is due to a lack of consistent nomenclature among different studies, which makes it challenging to compare results. More importantly, though, is the fact that extant calculations do not encompass the full ranges of values for these five parameters that are relevant to experimental studies.

The recent study by Wilson and Coh partially addresses this situation by investigating τ_H and τ_E as a functions of the ep and ee scattering strengths and laser photon energy [42] over pertinent values. Overall, they show τ_H and τ_E can largely be characterized by the ratio of K_{ep} to K_{ee} , with some dependence upon $h\nu$. However, they limit their study to low excitation (small u_a) and a room temperature (RT) lattice ($T_p = 300$ K). Here we build upon this recent study—as well as the earlier

studies—in the following ways.

We begin by studying the structure of BTE scattering integrals (Sec. II). We see that the photon energy $h\nu$ is a natural energy normalizing factor for these integrals, which leads to a reduction in the number of key parameters from five to just three: a unitless ratio of ep to ee scattering β/δ , a unitless phonon temperature γ , and a unitless level of laser excitation α . This energy normalization subsequently leads to natural normalization of time: if any timescale is multiplied by either the normalized ep scattering strength β or the normalized ee scattering strength δ , then the resulting unitless timescale is a function of the scattering strengths only through the unitless scattering-strength ratio β/δ .

Before getting to our main results regarding distribution relaxation, we briefly discuss single-electron scattering times (Sec. III). This discussion allows us to clearly distinguish these single-particle times from the relaxation times τ_H , τ_E , and τ_{th} that describe evolution of the distribution function $f(\epsilon, t)$. We also briefly discuss the energy relaxation time τ_E^{th} for a hot thermal (FD) distribution, which is relevant to understanding τ_E for laser-pulse-excited distributions.

The core of the paper comprises our investigation of $f(\epsilon, t)$ and the associated distribution relaxation times τ_H , τ_E , and τ_{th} as functions of the three normalized parameters (Sec. IV). We study, first in the low-excitation limit (small α), the evolution of $f(\epsilon, t)$ over the complete range (0 to ∞) of β/δ . We do this for three different values of the normalized phonon temperatures γ . From our calculations of $f(\epsilon, t)$ we numerically derive values of τ_H , τ_E , and τ_{th} . The dependence of each (normalized) relaxation time on the ratio β/δ is clearly revealed, and for each we present a heuristic expression that accurately describes the β/δ dependence. The dependence of the three relaxation times is then investigated over ranges of β/δ and α appropriate to room-temperature ($T_p = 300$ K) experimental studies of ultrafast carrier dynamics in simple metals. The dependence of the relaxation times on α reveal three distinct dynamical regions: a low-excitation (α independent) region, an intermediate (transition) region, and a high-excitation region where the two-temperature (2T) model [49] of carrier dynamics is approximately valid. We find that most experimental studies reside in the intermediate excitation region.

A number of approximate relations for τ_E and τ_{th} appear in the literature [41–45]. As part of our discussion we re-express these relations in terms of our normalized parameters, which allows us to readily assess their accuracy via comparison with our numerical results.

II. BTE MODEL OF CARRIER EXCITATION AND RELAXATION

The derivation of our theoretical model, which we briefly review here, has been previously described in detail [50]. First, we assume excitation is uniform in space

so that carrier transport can be neglected. Second, the scattering integrals in the BTE are averaged over k space, which produces a formulation of the BTE that only depends upon the carrier energy ϵ ,

$$\frac{\partial f(\epsilon, t)}{\partial t} = \Gamma_{ep}[f] + \Gamma_{ee}[f] + \Gamma_{e\gamma}[f], \quad (1)$$

where the three terms on the right side of this equation are the electron-phonon (ep), electron-electron (ee), and

electron-photon ($e\gamma$) scattering integrals. The $e\gamma$ integral describes excitation by a laser source, while the ep and ee integrals describe subsequent relaxation of the carriers. Our general formulations of the scattering integrals depend upon averaged scattering strengths and the electronic density of states $g(\epsilon)$. Because for the sp metals of interest here $g(\epsilon)$ is largely featureless for several eV about the Fermi level, we simply assume $g(\epsilon) = g_0$ is constant. With these approximations the three scattering integrals can be expressed as

$$\Gamma_{ep}[f] = -K_{ep} \left\{ [2f(\epsilon) - 1] f'(\epsilon) - k_B T_p f''(\epsilon) \right\}, \quad (2)$$

$$\begin{aligned} \Gamma_{ee}[f] = & -K_{ee} \int d\epsilon_3 \int d\epsilon_4 \left(\{ f(\epsilon) f(\epsilon_3 + \epsilon_4 - \epsilon) [1 - f(\epsilon_3)] [1 - f(\epsilon_4)] \right. \\ & \left. - [1 - f(\epsilon)] [1 - f(\epsilon_3 + \epsilon_4 - \epsilon)] f(\epsilon_3) f(\epsilon_4) \right\}, \end{aligned} \quad (3)$$

and

$$\Gamma_{e\gamma}[f] = K_{e\gamma}(t) \left\{ f(\epsilon - h\nu) [1 - f(\epsilon)] - f(\epsilon) [1 - f(\epsilon + h\nu)] \right\}. \quad (4)$$

Equation (2) was derived under the additional assumption $k_B T_p \gtrsim \hbar\Omega$, where Ω is any phonon frequency. In our analysis we assume T_p does not vary in time. Additionally, the electron-photon integral assumes photon absorption is indirect [50], which is primarily applicable to intraband transitions.

A key quantity in our analysis is the rate of energy transfer from the excited carriers to the phonons. This is obtained from the ep scattering integral [Eq. (2)] and can be written as [50]

$$\frac{d\langle\epsilon\rangle}{dt} = -K_{ep} g_0 \int d\epsilon \left\{ f'(\epsilon) k_B T_p + f(\epsilon) [1 - f(\epsilon)] \right\}, \quad (5)$$

If the excited carriers are internally thermalized—so that they are described by a FD distribution with temperature T_e —then Eq. (5) simplifies to

$$\frac{d\langle\epsilon\rangle_{FD}}{dt} = -K_{ep} g_0 k_B (T_e - T_p). \quad (6)$$

This last relation is a key result of the 2T model of electron-phonon dynamics [49], where it is assumed that the electronic and vibrational subsystems are characterized by temperatures T_e and T_p , respectively.

The interaction strengths K_{ep} , K_{ee} , and $K_{e\gamma}$ are all related to physical quantities that have been characterized for many metals. The ep strength can be written as [50]

$$K_{ep} = \pi \hbar \lambda \langle \Omega^2 \rangle, \quad (7)$$

where

$$\lambda \langle \Omega^n \rangle = 2 \int d\Omega \alpha^2 F(\Omega) \Omega^{n-1}. \quad (8)$$

Here $\alpha^2 F(\Omega)$ is the ep spectral density function and $\lambda = \lambda \langle \Omega^0 \rangle$ is the mass enhancement factor from superconductivity theory. The ee scattering strength is related to the single-carrier ee scattering rate $1/\tau_{ee}$ via [43]

$$\frac{1}{\tau_{ee}(\delta\epsilon)} = \frac{K_{ee}}{2} (\delta\epsilon)^2, \quad (9)$$

where $\delta\epsilon = \epsilon - \epsilon_F$ is the energy of a carrier with respect to the Fermi energy ϵ_F . (This scattering rate is discussed in more detail in Sec. III A.) The excitation scattering strength $K_{e\gamma}(t)$ is a function of $h\nu$, the volume normalized density of states $g_v = g_0/V$ [$\text{J}^{-1}\text{m}^{-3}$], and the power density $p_d(t)$ [$\text{J s}^{-1}\text{m}^{-3}$] absorbed by the metal,¹

$$K_{e\gamma}(t) = \frac{p_d(t)}{(\hbar\nu)^2 g_v}. \quad (10)$$

Because our primary goal is to characterize relaxation of the carriers, we treat laser excitation as simply as possible: we assume (i) the laser pulse is infinitely short

¹ The time dependent $K_{e\gamma}(t)$ defined here differs from the constant $K_{e\gamma}$ given in Ref. [50]. For a constant density of states g_v the two quantities are related via $K_{e\gamma}(t) = K_{e\gamma} n_{h\nu}(t)/g_v$, where $n_{h\nu}(t)$ is a function proportional to the laser intensity. See Ref. [50] for further details.

and (ii) any given electron can only absorb one photon. This approximation decouples the excitation and relaxation processes, although—as we see below—relaxation is dependent upon both photon energy and laser excitation strength. We assume the pre-excitation carriers are characterized by a FD distribution $f_{FD}(\epsilon, T_p)$. It then follows that laser-pulse excitation produces the nascent distribution

$$f_n(\epsilon) = \alpha \left\{ 1 - f_{FD}(\epsilon - h\nu, T_p) [1 - f_{FD}(\epsilon, T_p)] - f_{FD}(\epsilon, T_p) [f_{FD}(\epsilon + h\nu, T_p)] \right\}, \quad (11)$$

which hence is the initial distribution for the BTE driven solely by ep and ee scattering. Here

$$\alpha = \int K_{e\gamma}(t) dt = \frac{u_d}{(h\nu)^2 g_v} = \frac{n_e}{h\nu g_v}, \quad (12)$$

where n_e [m^{-3}] is the density of excited carriers. Because α is unitless, it is a natural descriptor for the carrier excitation level. As we see below, α ($-\alpha$) is (essentially) the laser induced change in f above (below) ϵ_F at energies $|\delta\epsilon| < h\nu$.

Because the photon energy $h\nu$ sets the range of energies over which the distribution is initially excited and because (typically) $h\nu \gg k_B T_p$, it is natural (and quite convenient) to normalize any energy quantities by $h\nu$. Doing so yields the normalized interaction strengths

$$\beta = \frac{K_{ep}}{h\nu} \quad (13)$$

and

$$\delta = K_{ee}(h\nu)^2, \quad (14)$$

and the normalized phonon and electron temperatures

$$\gamma = \frac{k_B T_p}{h\nu}, \quad \gamma_e = \frac{k_e T_e}{h\nu}. \quad (15)$$

Notice the normalized ep and ee strengths β and δ have the same units [s^{-1}]. These normalized quantities thus provide a natural (unitless) descriptor for the ratio of ep to ee interaction strengths,

$$\frac{\beta}{\delta} = \frac{K_{ep}}{K_{ee}(h\nu)^3}. \quad (16)$$

We use this ratio as the primary parameter in organizing our results below. Notice $\partial f(\epsilon, t)/\partial t$ is additive in K_{ep} and K_{ee} , and thus is additive in β and δ . Consequently, any timescale τ associated with $f(\epsilon, t)$ has the property that either (unitless combination) $\tau\beta$ or $\tau\delta$ is a function of β and δ *only* via the unitless interaction strength ratio β/δ .

So what values of the controlling parameters β/δ and α are germane to experimental conditions utilized in ultrafast investigations of simple metals? The answer is provided in Fig. 1, which plots concurrent values of α and

β/δ that apply to an extensive collection of experiments² on Cu, Ag, Au, and Al [17–26, 36, 40, 45, 52–101]. We note all of the represented experiments were performed on RT samples at excitation levels below the damage threshold. Because $\beta/\delta \sim (h\nu)^{-3}$, this ratio strongly depends upon the photon energy $h\nu$. Strikingly, ultrafast experiments on Au have been performed for photon energies from 0.42 to 5.0 eV, which corresponds to a range of β/δ from $\sim 3 \times 10^{-5}$ to $\sim 5 \times 10^{-2}$. As can also be deduced from Fig. 1, the excitation strength α experimentally ranges from $\sim 10^{-5}$ to a few times 10^{-1} . As our calculations reveal below, this range crosses over from the region where relaxation rates are independent of α (at lowest excitation levels) to a limit where the 2T model [49] is a reasonable approximation to the dynamics (at highest excitation levels).

III. CARRIER DYNAMICS TIMESCALES

The timescales important to carrier dynamics can be divided into two types: (i) those associated with scattering of individual carriers and (ii) those associated with relaxation of an excited distribution. In anticipation of analyzing the results for the relaxation of the nascent distribution $f_n(\epsilon)$ in Sec. IV, here we discuss several of these timescales. A point of emphasis is the relationship between these timescales and the two material constants— K_{ep} and K_{ee} —that govern the strength of each type of scattering. We also offer a physical interpretation of the normalized scattering-strength ratio β/δ .

A. Single-carrier timescales

Here we consider both ep and ee scattering of a singly excited carrier. We assume the initial energy $\epsilon = \epsilon_F + \delta\epsilon$ of the carrier is such that $\delta\epsilon \gg k_B T_p$ and $\delta\epsilon \gg \hbar\Omega$. Under these conditions any possible final state resulting from ep scattering (with energy $\epsilon \pm \hbar\Omega$) will initially be empty. Regarding ee scattering of this single electron, the condition $\delta\epsilon \gg k_B T_p$ enables the approximation $T_p = 0$, in which case all possible final states are at energies between ϵ_F and $\epsilon_F + \delta\epsilon$, and these states are also initially empty.

The first relevant single-carrier time is the spontaneous phonon-emission time [41]

$$\tau_{ep}^0 = \frac{1}{\pi\lambda(\Omega)}, \quad (17)$$

which is related to the ep interaction strength K_{ep} [see

² Details of the experiments represented in Fig. 1 can be found in the Supplemental Material [51].

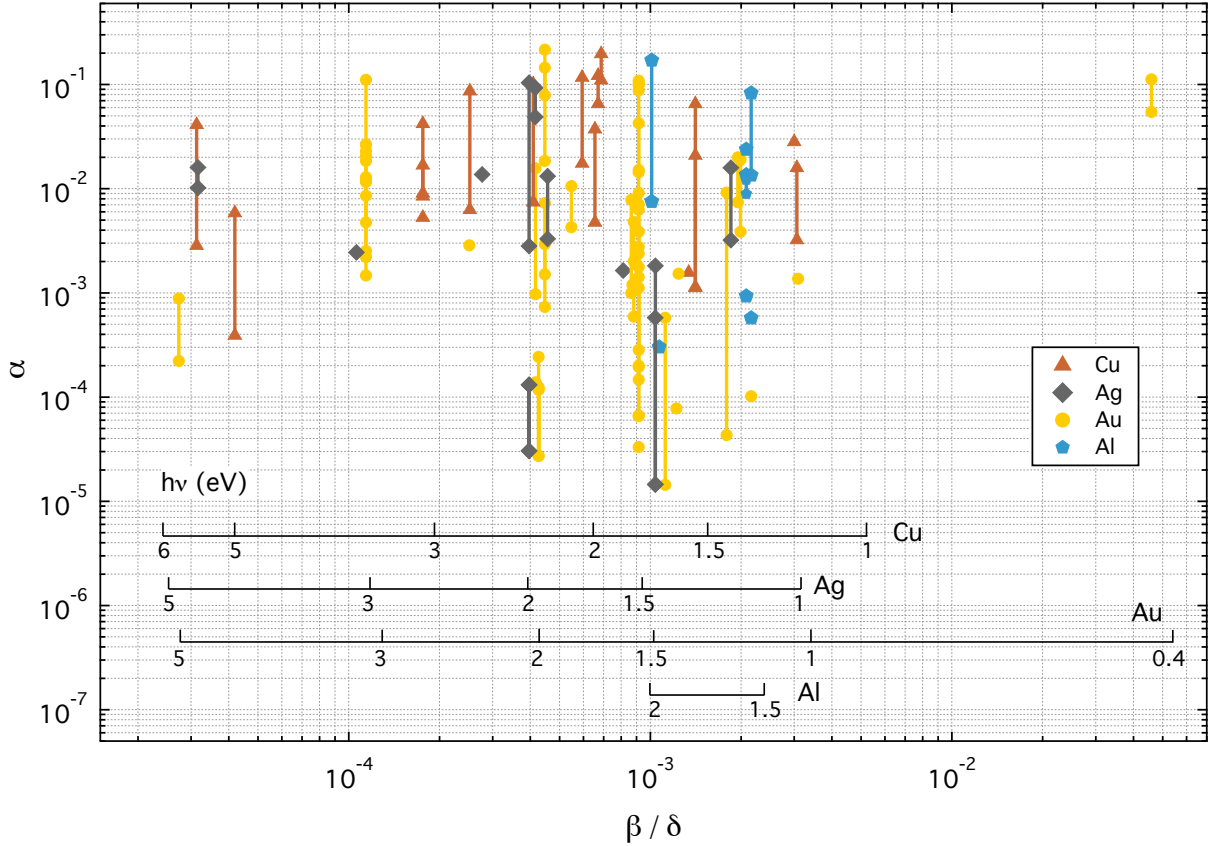


FIG. 1. Concurrent values of normalized excitation level α and normalized ratio of ep to ee coupling strengths $\beta/\delta = K_{ep}/[K_{ee}(h\nu)^3]$ in sub-damage-threshold RT experimental measurements (from the literature) on Cu, Ag, Au, and Al. Each set of two markers connected by a vertical line indicate the range of α for a particular experiment. Experiments that involve only one excitation level are indicated by a single marker. The individual $h\nu$ axes for the four metals indicate the laser-pulse photon energy used in each experiment.

Eq. (7)] via

$$\tau_{ep}^0 = \frac{\hbar\bar{\Omega}}{K_{ep}}, \quad (18)$$

where $\bar{\Omega} = \langle\Omega^2\rangle/\langle\Omega\rangle$ is the scattering-strength-weighted average phonon frequency [see Eq. (8)]. The scattering strength K_{ep} thus has a key interpretation: because one phonon is spontaneously emitted at the rate $1/\tau_{ep}^0$, the average energy-loss rate \dot{q}_0 for a singly excited electron is simply

$$\dot{q}_0 = K_{ep}. \quad (19)$$

In Table I we list values of K_{ep} and τ_{ep}^0 for a selection of simple metals. These calculations require three parameters— λ , $\langle\Omega\rangle$, and $\langle\Omega^2\rangle$ —for any given metal. For λ we use the recommended values tabulated by Grimvall [102]. We estimate the values of $\langle\Omega\rangle$ and $\langle\Omega^2\rangle$ using $\langle\Omega\rangle = \frac{2}{3}(k_B\hbar)\Theta_{-1}$ and $\langle\Omega^2\rangle = \frac{1}{2}(k_B/\hbar)^2\Theta_{-1}\Theta_1$; here Θ_m is the m^{th} -moment Debye temperature [50]. For all but Ag, we obtain values of Θ_m from Wilson [103]. The values for Ag are derived from an analysis of the

phonon spectra of Kamitakahara and Brockhouse [104] by Antonov *et al.* [105]. As the results in Table I show, K_{ep} ranges from $\sim 5 \times 10^{-3}$ to ~ 1 meV/fs, while τ_{ep}^0 lies between ~ 20 and ~ 600 fs.

The second relevant single-carrier time is the total ep scattering time [102, 106]

$$\tau_{ep}(T_p) = \frac{\hbar}{2\pi\lambda k_B T_p}, \quad (20)$$

which in terms of K_{ep} can be written as

$$\tau_{ep}(T_p) = \frac{\hbar^2\langle\Omega^2\rangle}{2K_{ep}k_B T_p}. \quad (21)$$

In Table I we also include values for this scattering time for $T_p = 300$ K for the indicated metals. As shown there, $\tau_{ep}(300\text{ K})$ lies between ~ 10 fs and 30 fs.

We point out a key feature common to both τ_{ep}^0 and $\tau_{ep}(T_p)$. In contrast to K_{ep} , which is proportional to $\lambda\langle\Omega^2\rangle$, the scattering rates $1/\tau_{ep}^0$ and $1/\tau_{ep}(T_p)$ are proportional to $\lambda\langle\Omega\rangle$ and $\lambda\langle\Omega^0\rangle (= \lambda)$, respectively [see Eqs. (17) and (20)]. However, Eq. (10) for $(\partial f/\partial t)_{ep}$

simply involves $K_{ep} \sim \lambda(\Omega^2)$, sans any other moments of Ω . Therefore, neither of these two single-particle scattering times is fundamentally related to relaxation of the distribution function $f(\epsilon)$.

We now turn our attention to ee scattering. For a single electron initially in a state with energy $\epsilon = \epsilon_F + \delta\epsilon$ above a zero-temperature Fermi sea the ee scattering rate of this carrier is given by Eq. (9). Owing to our interest in the early-time decay of a laser excited solid—with excitation energies on the order of an eV—in Table I we compile values of $\tau_{ee}(1\text{ eV})$ for each of the metals, and from these values we use Eq. (9) to calculate the likewise listed K_{ee} values.

We determine these values of $\tau_{ee}(1\text{ eV})$ in two different ways, depending upon the metal in question. For Cu, Ag, Au, and Al, $\tau_{ee}(\delta\epsilon)$ has been experimentally assessed via time-resolved two-photon photoemission (TR2PPE) measurements [107]; values of $\tau_{ee}(1\text{ eV})$ are extracted from these measurements for these metals. No such data have been reported for the alkali metals. For estimating $\tau_{ee}(1\text{ eV})$ for these metals we turn to the Fermi-liquid-theory (FLT) expression of Pines and Nozieres for the ee scattering rate [108],

$$\frac{1}{\tau_{ee}(\delta\epsilon)} = \frac{\sqrt{3}\pi^2\omega_p}{128} \left(\frac{\delta\epsilon}{\epsilon_F}\right)^2. \quad (22)$$

Here ω_p is the plasma frequency. Using theoretical bandstructure derived values of ω_p and ϵ_F for the alkali metals [109], we calculate the values of $\tau_{ee}(1\text{ eV})$ listed in Table I.

Interestingly, Ag and Au have the weakest ee scattering, with the smallest values of $K_{ee} \approx 0.03\text{ eV}^{-2}\text{s}^{-1}$ and concomitantly $\tau_{ee}(1\text{ eV}) \approx 70\text{ fs}$. This weak scattering has been attributed to strong screening of the $n\text{ sp}$ ($n = 5$ or 6) valence electrons by the rather delocalized $(n-1)d$ electrons [107]. Conversely, the two heaviest alkali metals (Rb and Cs) have the strongest ee scattering with $K_{ee} \approx 0.4\text{ eV}^{-2}\text{s}^{-1}$, resulting in $\tau_{ee}(1\text{ eV}) = 5\text{ fs}$. From the point of view of FLT, this strong scattering can be traced to the relatively small values of ϵ_F for these two metals.

Insight into the normalized scattering strength ratio β/δ is provided by considering the effects of each scattering process on the average energy-loss rate of a singly excited electron. Let us assume such an electron has excess energy $\delta\epsilon$ equal to a photon energy $h\nu$. If it were subject to only ee scattering, then it can be shown its initial average energy-loss rate is given by $\dot{q}_{ee} = K_{ee}(h\nu)^3/3$. Conversely, if this carrier were subject to only ep scattering, then its average energy-loss rate would be $\dot{q}_{ep} = K_{ep}$ [see Eq. (19)]. The ratio of these two rates is simply $\dot{q}_{ep}/\dot{q}_{ee} = 3\beta/\delta$. The ratio β/δ thus gives some measure of the relative effectiveness of the two scattering processes in decreasing the energy of any single carrier within a laser excited distribution.

In most cases the ratio β/δ is quite small. As shown in Table I, for $h\nu = 1.5\text{ eV}$ the values of β/δ are all less

than 3×10^{-3} . Similarly, Fig. 1 shows for Cu, Ag, Au, and Al that in nearly all experiments $\beta/\delta \lesssim 3 \times 10^{-3}$ (the exception being the experiment on Au with $h\nu = 0.42\text{ eV}$, for which β/δ is significantly larger but still < 0.1). Such small β/δ values indicate that ee scattering is the dominant contributor in relaxing the high energy end of a (typical) laser excited distribution. Indeed, this is quantitatively born out in our calculations of the hot-carrier relaxation time τ_H , reported in Sec. IV A 2.

B. Thermalized-distribution relaxation

Our discussion in Sec. IV focuses on relaxation times associated with the nascent (just after laser excitation) distribution given by Eq. (11). To appreciate those results, however, it behooves us to first consider the dynamics of a thermal (FD) distribution of carriers, which are characterized by an electron temperature T_e . In particular, here we look at the energy relaxation time τ_E^{th} of a FD distribution described by the electron temperature T_e . This relaxation time is defined via the relation $1/\tau_E^{th} = -(d\langle\epsilon\rangle/dt)/\langle\epsilon\rangle$, where $\langle\epsilon\rangle$ is the excess energy in the carriers. In terms of K_{ep} this time can be written as [106]

$$\tau_E^{th}(T_e, T_p) = \frac{\pi^2 k_B(T_e + T_p)}{6 K_{ep}}. \quad (23)$$

For high excitation levels where $T_e \gg T_p$ this relaxation time is not constant, as T_e varies in time. Therefore, energy decay is generally nonexponential. However, in the low-excitation limit, where $T_e \approx T_p$, Eq. (23) simplifies to

$$\tau_E^{th}(T_p) = \frac{\pi^2 k_B T_p}{3 K_{ep}}, \quad (24)$$

in which case the decay is well approximated by a simple exponential (under the constant- T_p approximation assumed here). As expected—and as opposed to the single-particle times τ_{ep}^0 and $\tau_{ep}(T_p)$ —this distribution-associated timescale depends upon the phonon spectrum solely through $K_{ep} \sim \lambda(\Omega^2)$ (and no other moments of Ω). In Table I we list values of $\tau_E^{th}(300\text{ K})$ as given by Eq. (24) for all of the considered metals. Although λ has some influence, the dramatic range of τ_E^{th} values is largely a consequence of K_{ep} being proportional to $\langle\Omega^2\rangle$.

In order to coherently organize the set of scattering times presented in Table I, we plot in Fig. 2 τ_{ep}^0 , $\tau_{ep}(300\text{ K})$, and $\tau_E^{th}(300\text{ K})$ vs $\tau_{ee}(1\text{ eV})$. For reference, $\tau_{ee}(1\text{ eV})$ is also plotted against itself. Because $\tau_E^{th}(300\text{ K})$ is the largest of all of these timescales, we have normalized all of the scattering times by this relaxation time. As can be seen in the figure (or deduced from Table I), the three ep driven timescales are related by the condition

$$\tau_{ep}(300\text{ K}) < \tau_{ep}^0 < \tau_E^{th}(300\text{ K}) \quad (25)$$

TABLE I. Material parameters and resulting ep and ee interaction parameters for several simple metals. The mass enhancement factor λ and phonon-frequency moments $\langle\Omega\rangle$ and $\langle\Omega^2\rangle$ are used as input parameters for calculating τ_{ep}^0 and τ_{ep} (the spontaneous-emission and total ep single-carrier scattering times, respectively), the ep coupling strength K_{ep} , the thermalized-distribution energy relaxation time τ_E^{th} , and the number of phonons N_{ph} emitted during the time τ_E^{th} . The ee scattering time τ_{ee} (at an excitation energy $\delta\epsilon = 1$ eV) is used as input to calculate the ee scattering strength K_{ee} . The ratio $\beta/\delta = (K_{ep}/K_{ee})(h\nu)^{-3}$ is the normalized ratio of ep to ee scattering strengths (here tabulated for photon energy $h\nu = 1.5$ eV).

Metal	λ^a	$\hbar\langle\Omega\rangle^b$ (meV)	$\hbar\langle\Omega^2\rangle^{1/2}$ (meV)	K_{ep} (meV/fs)	τ_{ep}^0 (fs)	τ_{ep}^c (fs)	$\tau_E^{th\ d}$ (fs)	N_{ph}	K_{ee} (eV ⁻² fs ⁻¹)	τ_{ee}^e (fs)	β/δ^f (10 ⁻⁶)
Li	0.40	19.9	22.2	0.940	26	10	91	2.5	0.167	12	1660
Na	0.16	8.8	9.7	0.072	148	25	1190	5.8	0.292	7	73
K	0.13	5.3	5.8	0.021	305	31	4050	9.6	0.359	6	17
Rb	0.16	3.3	3.6	0.010	400	25	8490	15.3	0.426	5	7
Cs	0.15	2.3	2.6	0.005	608	27	18200	21.6	0.423	5	3
Cu	0.15	18.0	19.1	0.262	78	27	325	3.0	0.050	40	1550
Ag	0.13	11.6	12.5	0.098	139	31	872	4.5	0.031	65	940
Au	0.17	9.7	10.7	0.092	127	24	923	5.2	0.027	75	1020
Al	0.43	21.0	22.8	1.071	23	9	79	2.5	0.133	15	2380

^a Reference [102].

^b See text for sources of $\langle\Omega\rangle$ and $\langle\Omega^2\rangle$.

^c at $T_p = 300$ K.

^d in the low excitation limit at $T_p = 300$ K.

^e at $\delta\epsilon = 1$ eV.

^f for $h\nu = 1.5$ eV.

for all of the metals listed. Furthermore, we see that the ratio of ee to ep rates is quite different for the four heaviest alkali metals in comparison with the Li, the noble metals, and Al.

Recognizing that the relationship between $\tau_{ep}(300\text{ K})$ and $\tau_E^{th}(300\text{ K})$ is typically a strong inequality—i.e., $\tau_{ep}(300\text{ K}) \ll \tau_E^{th}(300\text{ K})$ —Allen remarked “Electron energy loss at high T by phonon emission is a multistep process.” [106] However, because $\tau_{ep}(300\text{ K})$ involves scattering events that include both phonon emission and absorption, this relationship is perhaps not as interesting as that between τ_{ep}^0 and $\tau_E^{th}(300\text{ K})$, owing to τ_{ep}^0 being directly related to the energy-loss rate $\dot{q}_0 = K_{ep}$ of a singly excited carrier [see Eq. (18)].

However, an even better connection between relaxation at the single-carrier and the thermalized-distribution levels comes about by considering the average energy-loss rate \dot{q}_{th} for a single carrier that is itself part of the thermal distribution. As we now show, $\dot{q}_{th} \neq \dot{q}_0$. Because \dot{q}_{th} is equal to $-(d\langle\epsilon\rangle/dt)/N_{ex}$, we need the number of excess excitations (both electrons and holes)

$$\begin{aligned} N_{ex} &= 2g_0 \int_{\epsilon_F}^{\infty} [f_{FD}(\epsilon, T_e) - f_{FD}(\epsilon, T_p)] d\epsilon \\ &= 2\ln(2)g_0k_B(T_e - T_p), \end{aligned} \quad (26)$$

and the thermalized-distribution energy-loss rate given by Eq. (6). We hence obtain

$$\dot{q}_{th} = \frac{K_{ep}}{2\ln(2)} = \frac{\dot{q}_0}{2\ln(2)}. \quad (27)$$

Thus, for a carrier in a thermalized distribution the ef-

fective spontaneous phonon-emission time is

$$2\ln(2)\tau_{ep}^0 \approx 1.39\tau_{ep}^0. \quad (28)$$

That this time constant is longer than that for a singly excited carrier is not surprising, as not all possible final states are initially empty for an electron within a FD distribution. Succinctly put, Pauli blocking slows down the energy decay rate compared to that for a singly excited electron. It appears that this difference between \dot{q}_0 and \dot{q}_{th} has not always been recognized [41, 45].

The ratio of Eq. (24) to Eq. (28) provides the answer to an interesting question: how many phonons N_{ph} are emitted (on average) by each carrier within an energy-decay time of the distribution? Indeed, in the low-excitation limit this number is identically this ratio,

$$N_{ph} = \frac{\tau_E^{th}(T_p)}{2\ln(2)\tau_{ep}^0} = \frac{\pi^2}{6\ln(2)} \frac{k_B T_p}{\hbar\Omega}. \quad (29)$$

In Table I we tabulate this quantity for $T_p = 300$ K. As Eq. (29) shows, the range of N_{ph} values simply reflects the variation of characteristic phonon frequencies across this range of metals.

IV. DISTRIBUTION RELAXATION

We now report results pertaining to relaxation of a laser excited carrier distribution, calculated using the model described in Sec. II. As discussed there, our calculations are aimed at quantitatively discerning how the

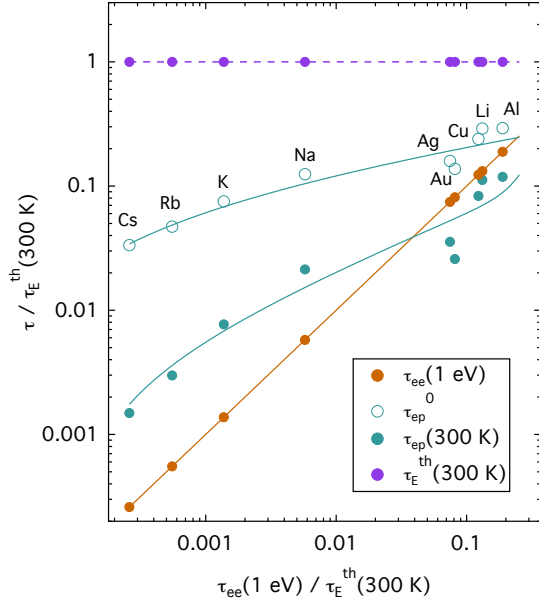


FIG. 2. Relaxation times relevant to excited carrier dynamics for the metals in listed in Table I. The time $\tau_{ee}(1\text{ eV})$ is the single-carrier ee scattering time for a carrier 1 eV above the Fermi energy, τ_{ep}^0 is the spontaneous phonon-emission scattering time, and $\tau_{ep}(300\text{ K})$ is the total ep scattering time at $T_p = 300\text{ K}$. All times are normalized to the thermalized-distribution energy relaxation time $\tau_E^{th}(300\text{ K})$. Solid lines are guides to the eye.

relative strength β/δ of ep to ee scattering, relative phonon temperature γ , and excitation level α govern the dynamics. As we shall see, for typical experimental conditions the metals in Table I are characterized by moderate to strong ee scattering or—equivalently—by weak to moderate ep scattering. Furthermore, we derive phenomenological expressions for timescales related to (i) hot-carrier relaxation (τ_H), (ii) energy transfer from the excited carriers to the phonon subsystem (τ_E), and (iii) thermalization of the nascent distribution (τ_{th}) that provide insight into the dynamics.

A. Low-excitation limit

In this section we study carrier relaxation in the low-excitation limit. Specifically, our results here are for $\alpha = 10^{-5}$ and values of γ equal to 0.0086, 0.0172, and 0.0344. These γ values were chosen because for $h\nu = 1.5\text{ eV}$ (a typical Ti:Al₂O₃ laser photon energy) and $T_p = 300\text{ K}$, we have $\gamma = k_B T_p / h\nu = 0.0172$. The other two values of γ thus correspond to the same photon energy with T_p equal to either 150 or 600 K. (Note however, these results also correspond any combination of T_p and $h\nu$ with the same ratios.) We note for $\alpha = 10^{-5}$ and $\gamma = 0.0172$, if the initial distribution were thermalized, then its temperature T_e would only be 1.0% greater than T_p .

1. Relaxation of $f(\epsilon, t)$

We begin our discussion of $f(\epsilon, t)$ relaxation by first examining the two extremes: ee scattering only ($\beta = 0$) and ep scattering only ($\delta = 0$). Results for these two cases are illustrated in Fig. 3. Note that $\alpha = 10^{-5}$ is readily ascertained from the curves in the two panels via the large plateau in $f(\delta\epsilon, 0)$ at this value.

As has been noted in the literature [40–42, 45], a primary consequence of ee scattering is the creation of more excitations as the distribution initially relaxes. This behavior is manifest in part (a) of Fig. 3. Although $f(\delta\epsilon, t)$ initially decreases at the highest energies, it increases to a much greater extent at lower energies, owing to (further) excitation of carriers that are initially below ϵ_F . At the earliest times ($t\delta \lesssim 1$) the division between $f(\delta\epsilon, t)$ increasing and decreasing occurs at the energy $\delta\epsilon/(h\nu) = (3 - \sqrt{3})/2 \approx 0.634$ (see [51]); the vertical arrow in the figure marks this energy.

As is apparent in part (b) of Fig. 3, relaxation of the distribution under the sole influence of ep scattering is quite different from that due to ee scattering. The behavior of this distribution time series can be understood by recalling that a singly excited carrier loses energy at the rate $\dot{q} = K_{ep}$. Because $f \ll 1$ for $\delta\epsilon/h\nu \gtrsim 0.25$, each carrier in this part of the distribution also loses (on average) energy at this same rate. Therefore, to good approximation the excited part of the distribution uniformly moves to lower energy at exactly this rate. In terms of normalized quantities we have $\dot{q}/h\nu = K_{ep}/h\nu = \beta$. Therefore, at time $t\beta$ the top end of the distribution will roughly reside at $1 - t\beta$. This behavior, first noted by Gusev and Wright [41], is evident in the figure. Further details concerning ep driven relaxation are discussed in Appendix A.

The transition from dominant ee scattering to dominant ep scattering is illustrated in Fig. 4, which comprises a set of $f(\delta\epsilon, t)$ curves for β/δ ranging between 10^{-5} to 1. First, we note as a function of $t\delta$ (rather than $t\beta$), the sets of curves for $\beta/\delta = 10^{-5}$ and 10^{-4} are essentially identical to the curves in part (a) of Fig. 3. Thus, for values of $\beta/\delta \lesssim 10^{-4}$ ee scattering is the main driver of changes in f . Differences in behavior become apparent beginning with the $\delta/\beta = 10^{-3}$ curves: as δ/β increases from 10^{-3} to 10^{-1} the dominance of ee over ep scattering clearly diminishes, and by $\delta/\beta = 10^{-1}$ the effects of ep scattering are apparent as early as $t\delta = 1$ (or equivalently $t\beta = 0.1$). For $\beta/\delta = 1$ ep scattering is clearly dominant: these curves are nearly identical to those in part (b) of Fig. 3 where $\delta = 0$.

2. Relaxation times

We now investigate the three relaxation times τ_H , τ_E , and τ_{th} . Each time is determined via a suitable measure of our numerically calculated distribution functions

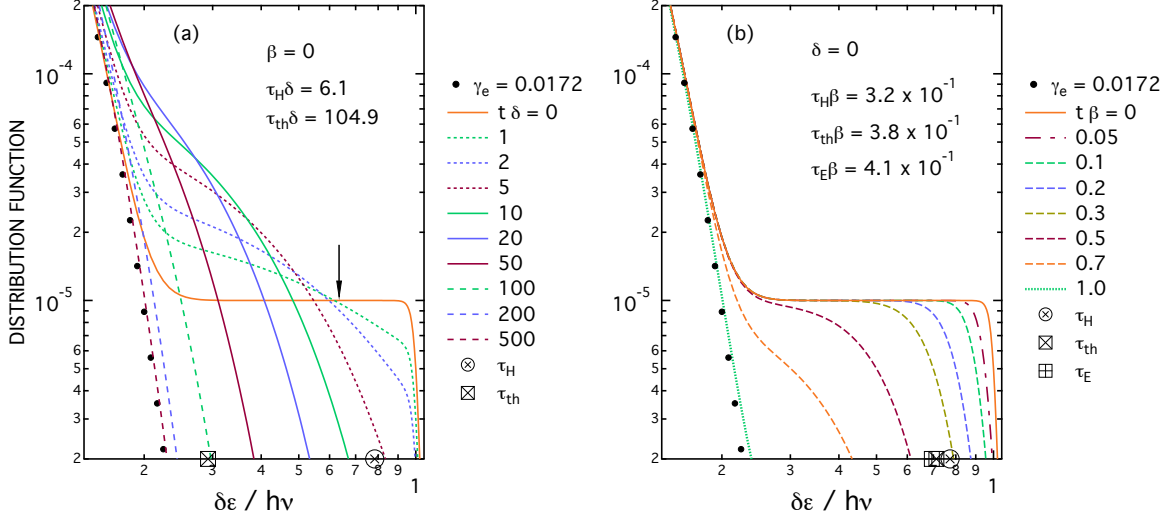


FIG. 3. Time series of (a) distribution function $f(\delta\epsilon, t)$ during relaxation for $\beta = 0$ (ee scattering only) and (b) during relaxation for $\delta = 0$ (ep scattering only). The vertical arrow in (a) is located at $\delta\epsilon/(h\nu) = (3 - \sqrt{3})/2$. Here the normalized excitation level and phonon temperature are $\alpha = 1 \times 10^{-5}$ and $\gamma = 0.0172$, respectively.

$f(\epsilon, t)$ (such as those shown in Figs. 3 and 4). In each case the relaxation time is defined to be the time it takes for its measure to decay to $1/e$ of its initial value (subsequent to laser-pulse excitation).

So what measures do we employ? For τ_H and τ_E they are quite simple (and identical to those used by Wilson

TABLE II. Relaxation times associated with hot electrons, energy, and thermalization in the strong ee and strong ep scattering limits at low excitation ($\alpha = 10^{-5}$). Analytic approximations in the strong ep scattering limit are indicated in the footnotes. For $h\nu = 1.5$ eV, the values of γ correspond to $T_p = 150, 300,$ and 600 K. Values of the Gusev and Wright thermalization time $\tau_{th}^G \delta$ are calculated using Eq. (42).

Relaxation times	$\gamma (= k_B T_p / h\nu)$		
	0.0086	0.0172	0.0344
Hot Electrons			
$\tau_H^{ee} \delta$	6.098	6.146	6.356
$\tau_H^{ep} \beta^a$	0.3162	0.3182	0.3275
Energy			
$\tau_E^{th} \beta$	0.0283	0.0566	0.1131
$\tau_E^{ep} \beta^b$	0.3966	0.4060	0.4233
$\tau_E^{ep} / \tau_E^{th}$	14.0	7.2	3.7
Thermalization			
$\tau_{th}^{ee} \delta$	365.2	104.9	31.83
$\tau_{th}^{ep} \beta^c$	0.3944	0.3848	0.3746
$\tau_{th}^G \delta$	679	170	43

^a Analytic approximation: $\tau_H^{ep} \beta = 0.3161$.

^b Analytic approximation: $\tau_E^{ep} \beta = 0.3935$.

^c Analytic approximations: $\tau_{th}^{ep} \beta = 0.3819, 0.3694,$ and 0.3415 for $\gamma = 0.0086, 0.0172,$ and 0.03444 , respectively.

and Coh [42]): the measure for τ_H is $N_{>h\nu/2}$, the number of excess carriers with energy $\delta\epsilon > h\nu/2$, and the measure for τ_E is $\langle \epsilon \rangle$, the excess energy in the carriers. Conversely, any measure that might be used to define τ_{th} is not so simple, owing to the need for some comparison between $f(\epsilon, t)$ and a thermal (FD) distribution $f_{FD}(\epsilon, T_e)$. A number of choices for this measure can be found in the literature, including (i) the number of excited carriers at small values of $\delta\epsilon$ ($\delta\epsilon \ll h\nu$) [43, 44, 65, 76], (ii) the energy per excited carrier [41], (iii) carrier entropy [48], and (iv) the rate of energy transfer from the carriers to the phonon subsystem [46]. Given that the degree of intracARRIER thermalization profoundly affects the transfer of energy from the electrons to the phonons, we define τ_{th} (in a manner similar to Rethfeld *et al.* [46]) via the rate of energy exchange between the carrier and phonon subsystems. Specifically, our measure is $|d\langle \epsilon \rangle / dt - d\langle \epsilon_{FD} \rangle / dt|$, the (magnitude of the) difference in the energy-exchange rates exhibited by the laser-excited nonequilibrium distribution and an *equal-energy* thermal distribution.

The time dependence of our three relaxation-time measures are illustrated in Fig. 5(a). Not unexpectedly, each measure decays in time toward zero. The dashed vertical line connected to each curve indicates when that measure has decayed to $1/e$ of its initial value, thence giving the associated relaxation time. Several properties exhibited by these curves are worth noting. (i) The ordering $\tau_H < \tau_{th} < \tau_E$ is exhibited for all cases studied at low excitation level. At high excitation levels we shall see that τ_{th} becomes smaller than τ_H . (ii) The curve for $\langle \epsilon \rangle$ vs t is clearly not exponential in nature. Although not obvious in the figure, this is also true of the thermalization measure. Decay of $N_{>h\nu/2}$ is typically quite close to exponential at low excitation, but becomes rather more complicated at high excitation. (iii) It is worth considering

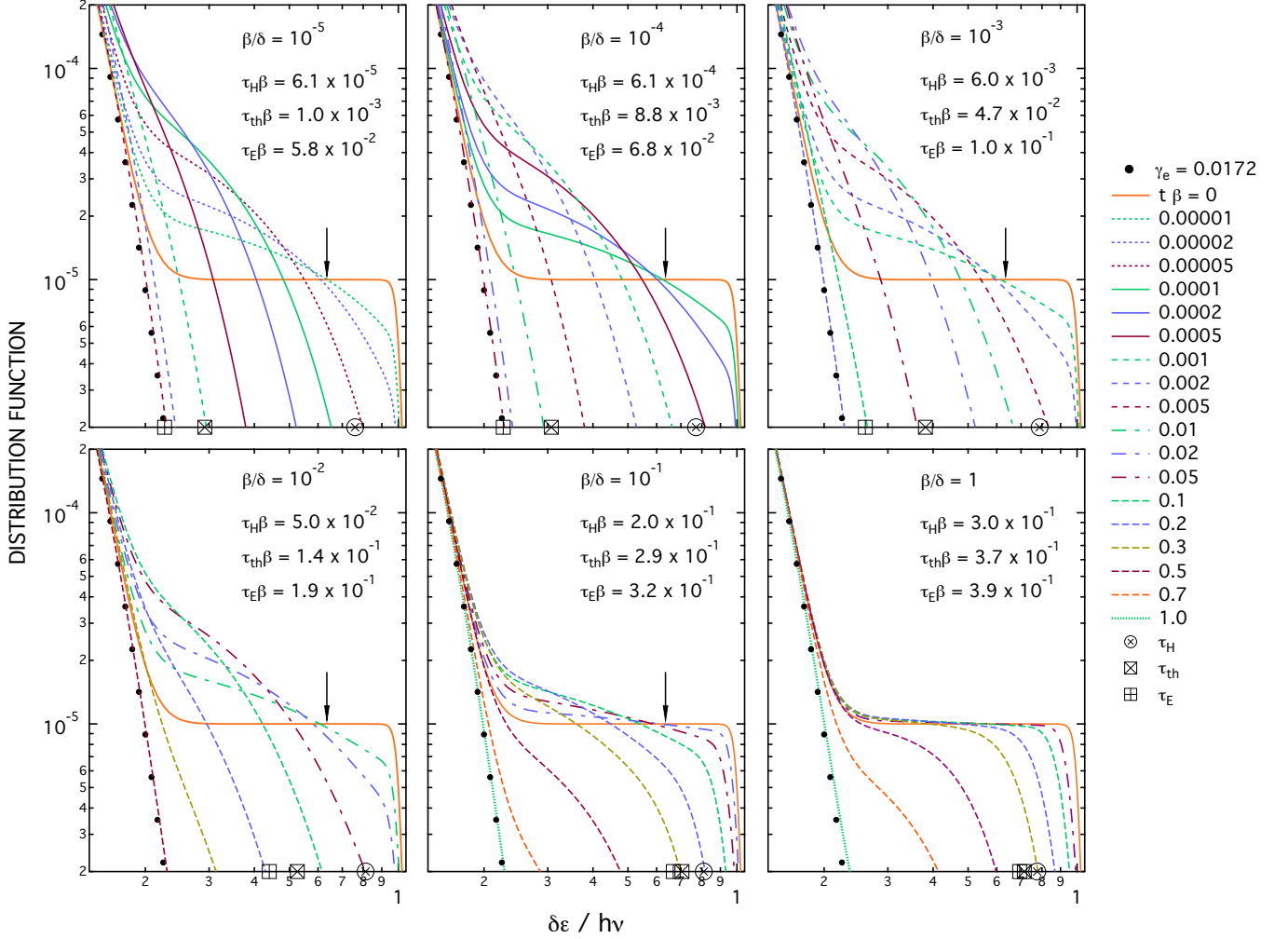


FIG. 4. Time series of laser-excited distributions $f(\delta\epsilon, t)$ during relaxation for six different values of the ratio β/δ of ep to ee interaction strengths. The vertical arrows are located at $\delta\epsilon/(h\nu) = (3 - \sqrt{3})/2$. Here the normalized excitation level and phonon temperature are $\alpha = 1 \times 10^{-5}$ and $\gamma = 0.0172$, respectively.

the two components associated with the degree of thermalization; these components are displayed in panel (b) of Fig. 5. Unsurprisingly, $-d\langle\epsilon_{FD}\rangle/dt$ decreases monotonically, consistent with the fact that this quantity monotonically increases as a function of $\langle\epsilon_{FD}\rangle$ [49]. That $-d\langle\epsilon\rangle/dt$ initially increases is due early-time dominance of ee scattering, which initially drives an increase in the number of carriers that are available to exchange energy with the phonons [39–42]. This comparison of $-d\langle\epsilon\rangle/dt$ and $-d\langle\epsilon_{FD}\rangle/dt$ also readily shows that several time constants must pass before the distribution is effectively thermalized.

An overview of our numerical results for the relaxation times is shown in Fig. 6, which plots values (normalized by β) for all three times as a function of β/δ . The left (right) side of the graph corresponds to relatively strong ee (ep) scattering. The vertical lines labeled with the set of sp metals indicate the corresponding β/δ values for $h\nu = 1.5$ eV. Only one curve for τ_H is shown, owing to

its extremely weak dependence upon γ (a consequence of $\gamma \ll 1/2$ for all three cases). As mentioned with regard to Fig. 5, the relation $\tau_H < \tau_{th} < \tau_E$ is exhibited by all of these data. In what follows we discuss each of these relaxation times in detail.

a. Hot-carrier relaxation

As can be inferred from Fig. 3, both ee and ep scattering contribute to the decrease in $N_{>h\nu/2}$, the number of carriers with energy $\delta\epsilon > h\nu/2$. As we now show, the contributions of the two scattering mechanisms are nearly independent of each other. Complete independence would be confirmed if the rate $1/\tau_H$ were to exhibit Matthiessen's rule, $1/\tau_H = 1/\tau_H^{ee} + 1/\tau_H^{ep}$, where here (and in subsequent relaxation-time expressions) the superscripts ee and ep indicate the limit of purely ee scattering or ep scattering, respectively. This relationship al-

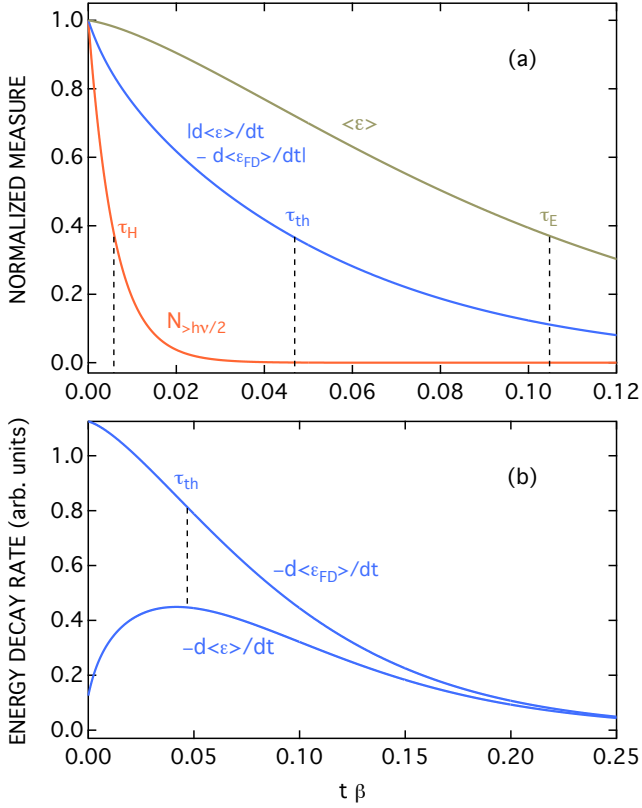


FIG. 5. Illustration of the measures for τ_H , τ_E , and τ_{th} . Each relaxation time is defined to be the time that its corresponding measure decays to $1/e$ of its initial value. For τ_H , τ_E , and τ_{th} these measures are $N_{>h\nu/2}$ (the number of carriers with energy $\delta\epsilon \geq h\nu/2$), $\langle\epsilon\rangle$ (the excess energy in the carriers), and $|d\langle\epsilon\rangle/dt - d\langle\epsilon_{FD}\rangle/dt|$ (the difference in energy loss rates between the laser excited distribution and an equal-energy FD distribution), respectively. Panel (a) shows the time dependence of each of these measures, with the corresponding τ indicated. Panel (b) separately shows the two energy decay rates $-d\langle\epsilon\rangle/dt$ and $-d\langle\epsilon_{FD}\rangle/dt$ used to determine τ_{th} . Here $\alpha = 10^{-5}$, $\beta/\delta = 10^{-3}$, and $\gamma = 0.0172$, which corresponds to the set of $f(\delta\epsilon, t)$ curves in the top right panel of Fig. 4.

most describes our data. However, we find that a slightly better description is given by an extended Matthiessen's rule,

$$\left(\frac{1}{\tau_H}\right)^a = \left(\frac{1}{\tau_H^{ee}}\right)^a + \left(\frac{1}{\tau_H^{ep}}\right)^a, \quad (30)$$

where from fitting we find an exponent $a = 0.95$.³ Values of $\tau_H^{ee}\delta$ and $\tau_H^{ep}\beta$ are given in Table II for the three values of γ investigated. As is evident there, both $\tau_H^{ee}\delta$ and $\tau_H^{ep}\beta$ are largely independent of γ . Indeed, all of the τ_H data

³ Analysis of the numerical τ_H data, as well as the τ_E and τ_{th} data, is described in detail in [51].

TABLE III. Distribution relaxation times τ_H , τ_{th} , and τ_E for the metals listed in Table I. Calculated times are for $h\nu = 1.5$ eV and $T_p = 300$ K ($\gamma = 0.0172$) at low excitation ($\alpha = 10^{-5}$). These times correspond to the solid curves in Fig. 6. Also tabulated are the ratios τ_H/τ_E , τ_E/τ_E^{th} , and τ_{th}/τ_E .

Metal	τ_H (fs)	τ_{th} (fs)	τ_E (fs)	τ_H/τ_E	τ_E/τ_E^{th}	τ_{th}/τ_E
Li	16	99	187	0.08	2.08	0.53
Na	9	140	1430	0.006	1.21	0.098
K	8	125	4370	0.002	1.08	0.028
Rb	6	107	8860	0.0007	1.04	0.012
Cs	6	109	18600	0.0003	1.03	0.006
Cu	53	343	662	0.08	2.04	0.52
Ag	87	691	1590	0.05	1.83	0.43
Au	100	770	1720	0.06	1.86	0.45
Al	19	105	179	0.11	2.26	0.58

are well described by the relation

$$\left(\frac{1}{\tau_H}\right)^{0.95} = \left(\frac{\delta}{6.2}\right)^{0.95} + \left(\frac{\beta}{0.32}\right)^{0.95}. \quad (31)$$

The result expressed by Eq. (31) is quite illuminating. First, from this equation we infer the contributions of the two scattering mechanism are equal at $\beta/\delta \approx 5 \times 10^{-2}$. Second, as shown by the β/δ locations of the seven metals in Fig. 6, we see for these (and the heavier alkali metals, see Table I) that ee scattering is the dominant relaxation mechanism associated with τ_H .

The strong ee scattering limit is thus interesting in its own right. First, we note $\tau_H^{ee}\delta \approx 6.2$ is in agreement with the results of Wilson and Coh [42]. Second, using Eqs. (9) and (14) it is trivial to show

$$\tau_H^{ee} = 3.1 \tau_{ee}(h\nu). \quad (32)$$

That is, in this limit the hot-electron relaxation time is only three times longer than the single-particle scattering time for the highest energy electrons in the distribution.

At the other extreme—dominant ep scattering—we have $\tau_H^{ep}\beta \approx 0.32$. As discussed in Appendix A, this result can be simply understood by solely considering the consequences of spontaneous phonon emission. Indeed, via an analytic calculation (see the appendix) we find $\tau_H^{ep} = (1 - 1/e)/2 = 0.3161$, which is remarkably close to the numerical results displayed in Table II.

Because $\beta/\delta \propto (h\nu)^{-3}$ [see Eq. (16)], the β/δ values associated with the seven metals indicated in Fig. 6 can be shifted parallel to the abscissa by changing $h\nu$. For example, a change in $h\nu$ from 1.5 eV (the value used in the figure) to 0.5 eV shifts the value of β/δ for Al from 2.4×10^{-3} to 6.5×10^{-2} . This change puts Al into the region where ep scattering very slightly dominates ee scattering in determining τ_H , but for the other metals in Fig. 5, τ_H is still primarily controlled by the ee interaction.

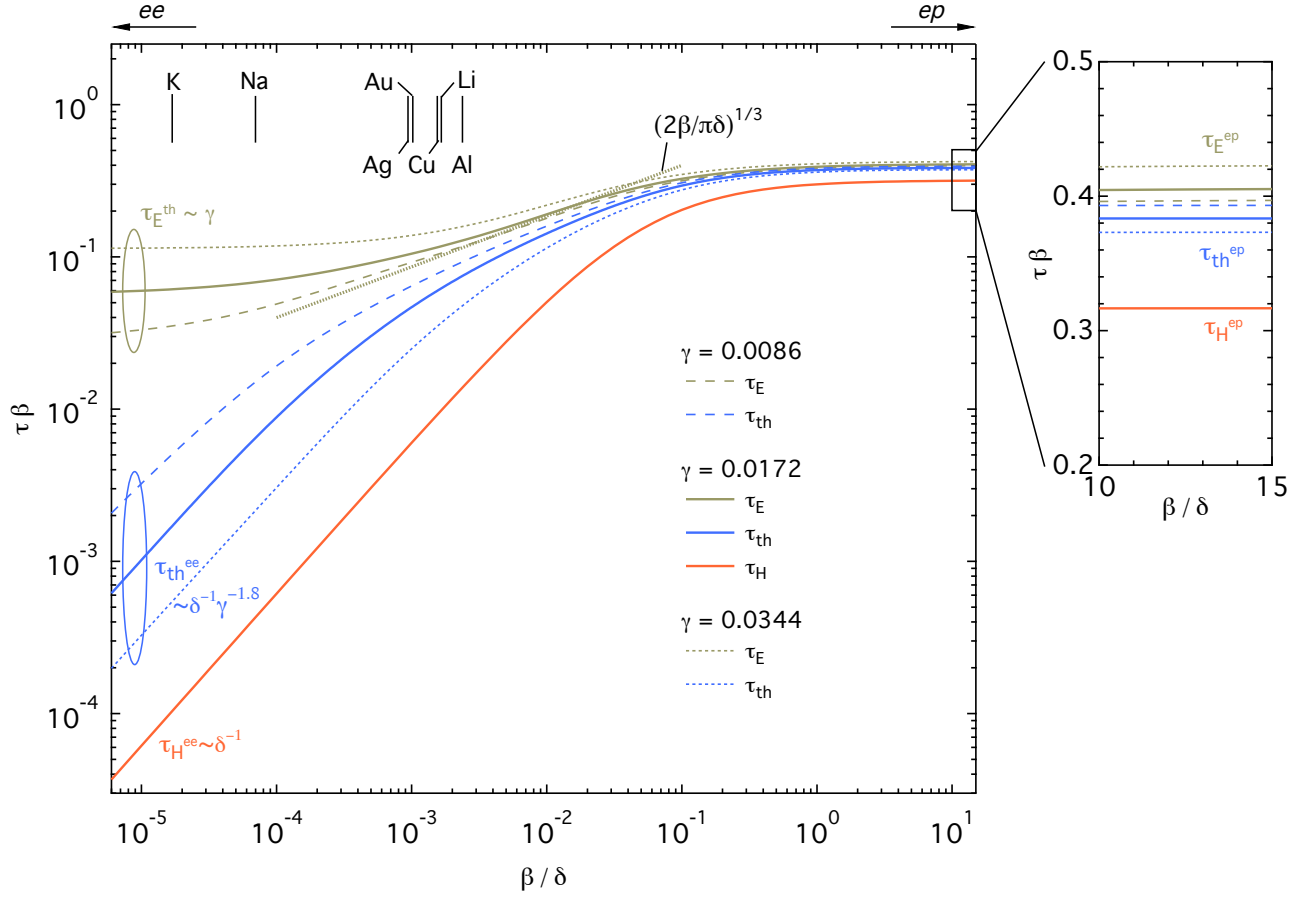


FIG. 6. (a) Normalized relaxation times $\tau_H\beta$, $\tau_{th}\beta$, and $\tau_E\beta$ vs ratio β/δ of ep to ee interaction strengths. Strong ee (ep) coupling is on the left (right) side of the main graph. The small graph to the right is a detailed look at the $10 < \beta/\delta < 15$ region. These results are at low excitation level ($\alpha = 1 \times 10^{-5}$), and the values of β/δ indicated for the seven metals are for photon energy $h\nu = 1.5$ eV. The dotted line labeled $(2\beta/\pi\delta)^{1/3}$ is the result $\tau_E^G\beta$ derived by Gusev and Wright [41].

To visually connect τ_H with the electron distributions shown in Fig. 3 and 4, we have indicated τ_H on these figures: on the abscissa of each graph we mark (using the symbol \otimes) the location where the distribution function at time $t = \tau_H$ crosses the abscissa. Because in all of these graphs $f = 2 \times 10^{-6}$ along the abscissa, this point is determined by the condition $f(\delta\epsilon, \tau_H) = 2 \times 10^{-6}$. As is evident, the energy of this point is universally quite close to $\delta\epsilon/h\nu = 0.8$.

Using these normalized results, we have calculated τ_H values for each of the metals listed in Table I. The results for τ_H for input parameters $h\nu = 1.5$ eV and $T_p = 300$ K ($\gamma = 0.0172$) are reported in Table III. As can be seen there, τ_H ranges from a few fs (for the four heaviest alkali metals) to 100 fs (for Au).

b. Energy relaxation

We now consider the energy relaxation time τ_E . A point of comparison is the relationship of τ_E to the energy-relaxation time τ_E^{th} of a thermalized (FD) distri-

bution. Because the present calculations are for very low excitation, the energy decay of a thermalized distribution is purely exponential, and so τ_E^{th} as given by Eq. (24) is the same as the $1/e$ decay time.

A comparative overview of τ_E and τ_E^{th} is provided by Fig. 7, which plots in each panel two energy-decay curves, one for a laser-excited distributions and one for a FD distribution with the same initial energy. The laser-excited decay curves correspond to the set of distributions in Fig. 4. Noting the horizontal dotted line in a panel in Fig. 7 marks the $1/e$ point for the energy remaining in the distribution, we readily observe (i) $\tau_E/\tau_E^{th} > 1$ and (ii) τ_E/τ_E^{th} increases as β/δ increases.

Our numerical results for τ_E vs β/δ are shown in Fig. 6. As the figure illustrates, each $\tau_E\beta$ curve has two clear asymptotic limits, with a halfway point close to $\beta/\delta = 10^{-2}$. As β/δ becomes increasingly smaller τ_E approaches τ_E^{th} [see Eq. (24)], which in normalized parameters can be expressed as

$$\tau_E^{th}\beta = \frac{\pi^2}{3}\gamma. \quad (33)$$

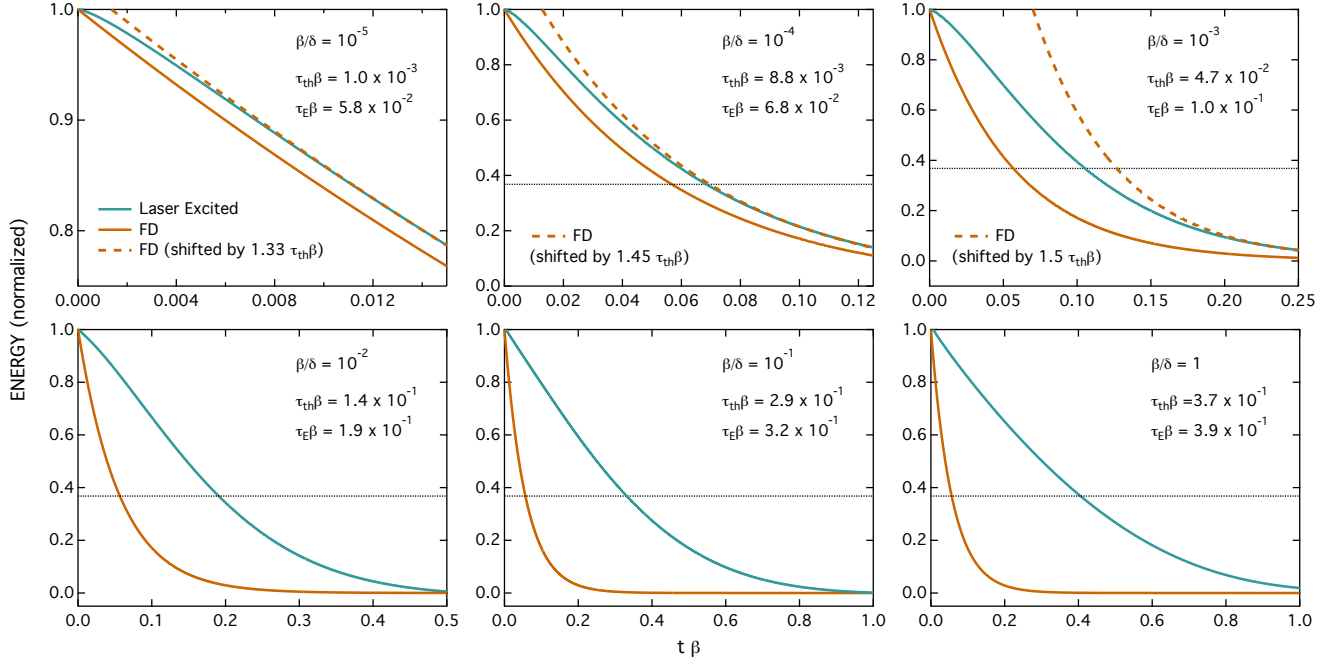


FIG. 7. Carrier energy vs time for six different values of the ratio β/δ of ep to ee interaction strengths. Each panel (as labeled by β/δ) corresponds to the analogous panel of Fig. 4. The energy decay for each laser-excited distribution is compared to the decay of a thermalized (FD) distribution. The dashed-line graph in the three top panels is the thermalized-distribution decay shifted by a small factor times $\tau_{th}\beta$. Energy is normalized to the initial energy in each distribution, and the horizontal dotted line marks $1/e$ on the energy axis. Here the normalized excitation level and phonon temperature are $\alpha = 1 \times 10^{-5}$ and $\gamma = 0.0172$, respectively.

In this very small β/δ regime ee scattering is so strong that the timescale τ_{th} for the distribution to become thermalized (which we discuss in detail shortly) is much shorter than the energy relaxation timescale τ_E . Therefore, energy transfer to the phonons essentially occurs from a thermalized carrier distribution. Consequently, in this regime the standard 2T model [49] is an excellent description of the energy dynamics. At increasingly larger values of β/δ —where ep scattering dominates—the second asymptote is approached. From our numerical calculations we find this limit is given by

$$\tau_E^{ep} \beta \approx 0.40. \quad (34)$$

More precise values of $\tau_E^{ep} \beta$ for each value of γ are given in Table II. We note those numerical results are quite close to the analytic approximation $\tau_E^{ep} \beta = 1 -$

$\sqrt{1/e} = 0.3935$, which is derived in Appendix A. The ratio $\tau_E^{ep}/\tau_E^{th} \approx 0.12/\gamma$ (values are tabulated in Table II) indicates the degree to which strong intraelectron thermalization enhances energy decay. This ratio is very nearly exhibited by the energy-decay curves in the $\beta/\delta = 1$ panel of Fig. 7.

We note the ee interaction does not appear (via δ) in either of the asymptotic-limit expressions for τ_E . At the smallest values of β/δ this occurs because the effects of ee scattering are over well before significant energy relaxation occurs. Conversely, in the large β/δ limit, any potential contribution from ee scattering is much too slow to impact relaxation of the energy.

We have developed a heuristic equation for τ_E that improves upon several equations offered by Wilson and Coh [42]. In our notation their most accurate expression (their Eq. S17) can be written as

$$\tau_E = \tau_E^{th} \left[1 + (A_0 + A_1 h\nu) \left\{ 1 - \tanh \ln (A_2 [(h\nu)^{2.86} K_{ee}/K_{ep}]^{0.42}) \right\} + [A_3 + A_4 (h\nu)^{1.1}] \operatorname{sech} \ln (A_5 [(h\nu)^{2.38} K_{ee}/K_{ep}]^{0.42}) \right], \quad (35)$$

where the A_i 's are fitted constants. There are two is-

issues with this equation. First, given the structure of the

BTE, the parameters $h\nu$, K_{ep} , and K_{ee} should appear together as the (unitless) combination $(h\nu)^3 K_{ee}/K_{ep}$ ($=\delta/\beta$). This combination almost appears correctly in the argument of the $\tanh \ln$ function, but in the $\text{sech} \ln$ function the combination is rather far off. Second, the other occurrences of $h\nu$ should appear divided by phonon temperature $k_B T_p$ (recall $h\nu/k_B T_p = \gamma^{-1}$). That $h\nu$ appears by itself in Eq. (35) can be attributed to the fact that Wilson and Coh only study materials at one temperature (RT). Our updated version of this equation—which we have used to fit our numerical data—is

$$\tau_E \beta = \frac{\pi^2}{3} \gamma \left[1 + (B_0 + B_1 \gamma^{-B_2}) \left\{ 1 - \tanh \ln (B_3 [\beta/\delta]^{-B_4}) \right\} + (B_5 + B_6 \gamma^{-B_7}) \text{sech} \ln (B_8 [\beta/\delta]^{-B_9}) \right]. \quad (36)$$

The best-fit values of the B_i 's are listed in Table IV. The typical deviation between the numerical data and Eq. (36) is $\sim 1\%$.

Aside from the analysis by Wilson and Coh, there has been one other expression previously offered for the energy relaxation time. From their analytic approximations Gusev and Wright [41] derive an expression for τ_E , which in our notation is given by

$$\tau_E^G \beta = \left(\frac{2\beta}{\pi\delta} \right)^{1/3}. \quad (37)$$

This relation is plotted in Fig. 6 as the dotted line labeled $(2\beta/\pi\delta)^{1/3}$. In the range of β/δ values germane to all but the four heaviest alkali metals, this expression is remarkably close to our numerical results for the smallest value of $\gamma = 0.0086$ (lowest temperature) we have studied. Furthermore, it reproduces in reasonable fashion the trend in $\tau_E \beta$ over the range $5 \times 10^{-4} < \beta/\delta < 5 \times 10^{-2}$. However, for the smallest values of β/δ (relevant to the heaviest alkali metals) this expression significantly underestimates τ_E . It also becomes less accurate as γ increases, in that the dependence of $\tau_E \beta$ upon β/δ increasingly deviates from a power law with exponent $1/3$. Indeed, for $\gamma = 0.0172$, the simple expression $\tau_E \beta \approx 0.66 (\beta/\delta)^{1/4}$ offered by Wilson and Coh is much more accurate for $5 \times 10^{-4} < \beta/\delta < 10^{-1}$ [42].

In Table III we also list values of τ_E for the simple metals. Like the τ_H values, these τ_E values are calculated using input parameters $T_p = 300$ K and $h\nu = 1.5$ eV. Most interesting is a comparison of τ_E and τ_E^{th} values, the latter quantity being the energy-decay time for an already thermalized distribution. The ratio of these two quantities is also reported in Table III. Excepting the four heaviest alkali metals, this ratio is close to 2, a consequence of the relatively slow intracARRIER thermalization (discussed in detail below) for these metals.

A comparison of τ_H and τ_E is also informative. (Here we also consider the specific case $\gamma = 0.0172$.) When $\beta/\delta \lesssim 10^{-4}$ we have $\tau_H/\tau_E \approx 100 \beta/\delta \lesssim 10^{-2}$. Therefore, for the four heaviest alkali metals hot-carrier relaxation is much faster than energy relaxation. For β/δ

TABLE IV. Best-fit values of the parameters B_i in Eq. (36).

i	B_i
0	-0.346314
1	0.059041
2	1.000961
3	0.232987
4	0.390694
5	-0.272834
6	0.004287
7	1.241227
8	0.116529
9	0.341017

values up to 2.5×10^{-3} we have $\tau_H/\tau_E \lesssim 0.1$. Thus, for all of the other metals in Table I hot-carrier relaxation is at least somewhat faster than energy relaxation (see Table III for specific ratio values). For $\beta/\delta \gtrsim 1$ (where ep scattering controls both relaxation times) the ratio is constant, with $\tau_H/\tau_E \approx 0.8$. That the ratio is close to unity is not surprising, owing to $\sim 3/4$ of the excess energy being initially contained in the hot electrons [those with $\delta\epsilon/(h\nu) > 0.5$]. The overall behavior of τ_H/τ_E vs β/δ is also evident in the distribution-function plots in Fig. 4, where τ_E is indicated (via the symbol \boxplus) in the same manner as τ_H .

c. Carrier thermalization

Along with the relaxation times τ_H and τ_E , our numerical results for τ_{th} are shown in Fig. 6. Not unexpectedly, for the smallest values of β/δ we have $\tau_{th} \ll \tau_E$. Importantly, as the normalized temperature parameter γ decreases these two relaxation approach each other. At the smallest values of β/δ this approach as a function of γ is dramatic, owing to $\tau_{th}^{ee}/\tau_E^{th} \sim \gamma^{2.8}$. (The dependence of τ_{th}^{ee} on γ is discussed in more detail below.)

At the extremes of β/δ the relaxation time τ_{th} has the same simple behavior as the hot-carrier relaxation time τ_H . For $\beta/\delta \lesssim 5 \times 10^{-5}$, τ_{th} is controlled by ee scattering and is given by

$$\tau_{th} \delta \approx \tau_{th}^{ee} \delta, \quad (38)$$

where the value of $\tau_{th}^{ee} \delta$ depends upon γ .⁴ Values of $\tau_{th}^{ee} \delta$ for the three values of γ studied here are given in Table II. Conversely, for $\beta/\delta \gtrsim 5 \times 10^{-1}$, τ_{th} is dominated by ep scattering. In this regime we have

$$\tau_{th} \beta \approx \tau_{th}^{ep} \beta \approx 0.38. \quad (39)$$

⁴ In the ee -only scattering limit, there is of course no energy transfer to the lattice, and so strictly speaking our thermalization measure $|d\langle\epsilon\rangle/dt - d\langle\epsilon_{FD}\rangle/dt|$ is undefined. However, at each time step of the calculation we can compare the requisite two relaxation rates by assuming an infinitesimal ep coupling.

More accurate values of $\tau_{th}^{ep} \beta$ are given in Table II, but as is evident there, $\tau_{th}^{ep} \beta$ is only weakly dependent upon γ . As we have done with τ_H and τ_E , we indicate τ_{th} (via the symbol \boxtimes) on the graphs in Figs. 3 and 4.

Given that τ_{th} is controlled by ee (ep) scattering at very small (large) values of β/δ , one might wonder if their contributions at intermediate values of β/δ are approximately independent, as is the case for τ_H . We have thus also fit this data with our power-law extension of Matthiessen's rule,

$$\begin{aligned} \left(\frac{1}{\tau_{th}}\right)^b &= \left(\frac{1}{\tau_{th}^{ee}}\right)^b + \left(\frac{1}{\tau_{th}^{ep}}\right)^b \\ &= \left(\frac{\delta}{\tau_{th}^{ee}\delta}\right)^b + \left(\frac{\beta}{\tau_{th}^{ep}\beta}\right)^b, \end{aligned} \quad (40)$$

where the constant values of $\tau_{th}^{ee}\delta$ and $\tau_{th}^{ep}\beta$ (for each value of γ) can be found in Table II. We find that Eq. (40) describe the data quite well for values of $\beta/\delta < 10^{-1}$, with best-fit value of the exponent b equal to 0.42, 0.52, and 0.66 for γ equal to 0.0086, 0.0172, and 0.034, respectively. Because b is not close to 1 for any of the cases, the two scattering mechanisms cannot be considered to be independent as far as thermalization is concerned. As is the case with energy relaxation, ee and ep scattering intertwine in a nontrivial manner to effect carrier thermalization. Unlike hot-carrier relaxation, however, the magnitude of the contribution from ep scattering to thermalization is quite important: for all but the four heaviest alkali metals, the thermalization rate is at least twice as fast as it would be if only ee scattering were operating. For Li and Al, for example, the thermalization rate is 2.8 and 3.3 times faster, respectively.

As β/δ increases beyond 10^{-1} we find that Eq. (40) with a constant value of b becomes increasingly poor at describing the dynamics. However, by allowing the exponent b to vary with β/δ as

$$b = \frac{b_0 + b_1 \beta/\delta}{1 + b_1 \beta/\delta} \quad (41)$$

a quite accurate description of the data is obtained for all values of β/δ . In Fig. 8 we plot fitted values of b as a function of β/δ .⁵ For $\beta/\delta \lesssim 5 \times 10^{-2}$, b is approximately constant (and nearly equal to the values obtained from the constant- b analysis above). However, a transition ensues in the range $5 \times 10^{-2} \lesssim \beta/\delta \lesssim 10$, above which the exponent is not far from 1. Hence, in the ep dominant region ($\beta/\delta \gtrsim 10$) the contributions of the two scattering mechanisms can be considered to be approximately independent.

Because rapid thermalization leads to efficient energy transfer, it is relevant to ask under what circumstances does thermalization precede significant energy

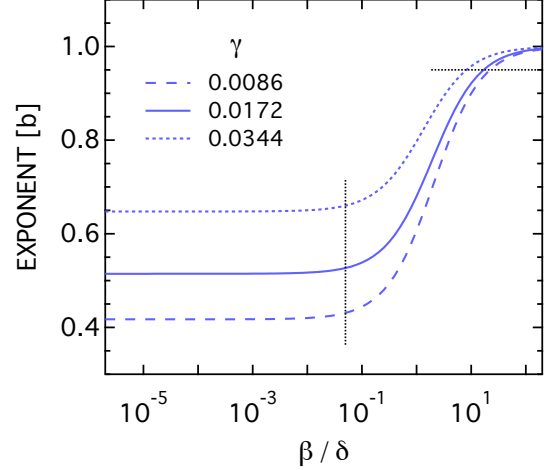


FIG. 8. Dependence of the thermalization time exponent b [see Eqs. (40) and (41)] on the ratio β/δ of ep to ee interaction strengths.

relaxation? To investigate this question we have again plotted in the top three panels of Fig. 7 the FD decay curve, but shifted in time by a small factor times $\tau_{th}\beta$. The small factor (1.33, 1.45, and 1.5 for $\beta/\delta = 10^{-5}$, 10^{-4} , and 10^{-3} , respectively) in each case is chosen so that the laser-excited and FD distribution curves overlap at later times. This comparison allow us to see that it is only for $\beta/\delta = 10^{-5}$ that this overlap occurs before substantial energy decay has occurred. Therefore, only for the $\beta/\delta \lesssim 10^{-5}$ data can we say that thermalization precedes energy relaxation. A comparison of the ratio τ_{th}/τ_E at $\beta/\delta = 10^{-5}$ and 10^{-4} is illuminating. The two ratios are 0.017 and 0.12, respectively. Thus, a ratio well under 0.1 is necessary for thermalization to precede energy decay.

Table III also reports values of τ_{th} , calculated using the same input parameters as τ_H and τ_E . Relevant to the present discussion we also tabulate the ratio τ_{th}/τ_E . For Rb and Cs this ratio 0.012 and 0.006, respectively. Thus the 2T model is applicable to these two metals. For K $\tau_{th}/\tau_E = 0.028$; the 2T model should thus be used with caution in this case. For all of the other metals the ratio is $\gtrsim 0.1$, which invalidates use of the 2T model to describe the dynamics. Our assessment agrees with the linearized BTE analysis of Baranov and Kabanov, who show that thermalization and energy decay happen on similar timescales in Au [44]. Pietanza *et al.* also note similar behavior at lower excitation levels in their BTE study of Ag [47].

Two sets of researchers offer simple expressions for τ_{th} when ee scattering dominates [41, 43, 44]. Gusev and Wright define a thermalization time to be the time when the average energy per excitation becomes equal to that

⁵ Fitted values of b_0 and b_1 are reported [51].

of a FD distribution [41].⁶ Written in our notation, their equation for τ_{th} is

$$\tau_{th}^G \delta = \left(\frac{2}{\pi}\right)^5 \left[\frac{\ln(2)}{\gamma}\right]^2 \approx \frac{1}{20\gamma^2}. \quad (42)$$

Kabanov and coworkers divide the excited carrier distribution into thermal and nonthermal parts [43, 44]. They consider relaxation of the nonthermal component and identify an asymptotic thermalization time τ_{th}^K . Specifically, they show at long times $[t/\tau_{th}^K \gg (1, \gamma^2)]$ the non-thermal component of the carrier density has the time dependence $e^{-t/\tau_{th}^K}/t$, where

$$\tau_{th}^K \delta = \frac{2}{\pi^2 \gamma^2} \approx \frac{1}{5\gamma^2}. \quad (43)$$

We note this relation has the same $1/\gamma^2$ dependence as Eq. (42), but is about four times longer. This difference can be attributed (at least in part) to the fact that at long times most of the electrons have relaxed to low-energy states ($\delta\epsilon \ll h\nu$), which have much reduced ee scattering rates.

Numerically we find the γ^{-2} behavior exhibited by Eqs. (42) and (43) is not quite obeyed. Our calculations instead reveal in the very strong ee scattering regime that the thermalization time is accurately described by the expression $\tau_{th}^{ee} \delta = 3.33 + 0.059\gamma^{-1.83}$. Interestingly, values calculated using the approximate Gusev and Wright relation Eq. (42) are within at least a factor of 2 of our numerical results, as can be seen by comparing the values of $\tau_{th}^{ee} \delta$ and $\tau_{th}^G \delta$ listed in Table II.⁷

B. Higher excitation levels

We now investigate carrier relaxation as a function of excitation level α . As we discuss in detail below, a transition region exists between the small α behavior discussed above and large α behavior (where the 2T model is a reasonable approximation). As far as we have been able to ascertain, our analysis is the first to identify and characterize this transition region.

For the following reasons, our α dependent calculations focus on Ag and Au. First, of all the simple metals, Au has been most extensively studied in the ultrafast time domain (this fact is reflected in the data plotted in Fig. 1). Second, the (unnormalized) ratio K_{ep}/K_{ee} of ep to ee scattering strengths is nearly the same for the two metals: $K_{ep}/K_{ee} = 3.17 \times 10^6 \text{ meV}^3$ and $3.46 \times 10^6 \text{ meV}^3$ for Ag and Au, respectively. We can thus simultaneously

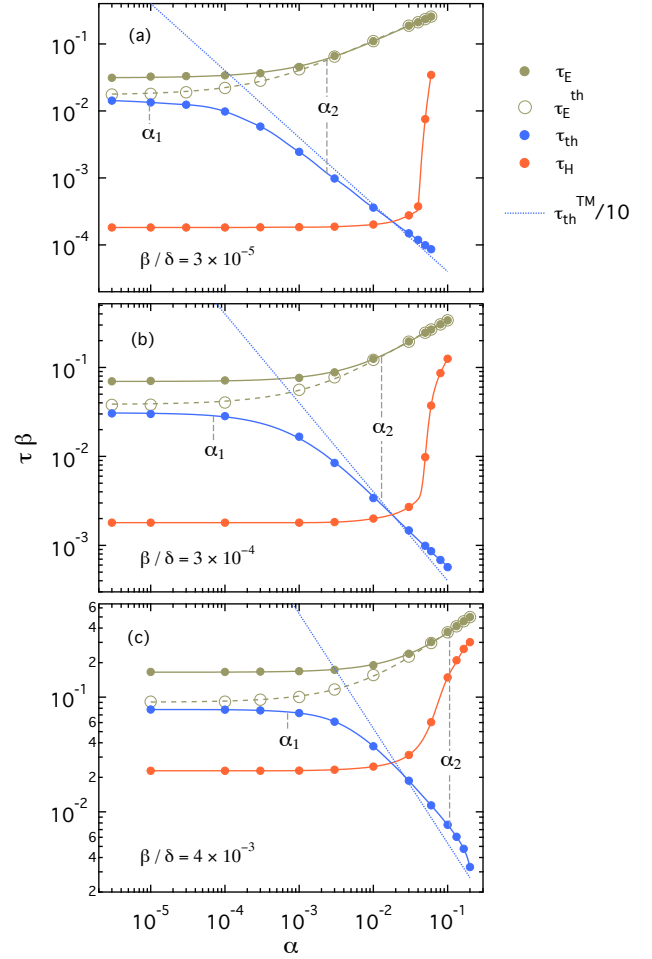


FIG. 9. Relaxation times τ_H , τ_{th} , τ_E^{th} , and τ_E in RT idealized Ag/Au vs excitation level α . Circles are calculated values, and curves are guides to the eye. Calculations for $\beta/\delta = 3 \times 10^{-5}$, 3×10^{-4} , and 4×10^{-3} (which correspond to $h\nu = 4.83$, 2.24, and 0.94 eV, respectively) are shown. The dotted blue lines are 1/10 of the Tas and Maris [45] thermalization time τ_{th}^{TM} [see Eq. (46)]. The boundaries α_1 and α_2 are defined by Eqs. (44) and (45), respectively.

model both metals in reasonable fashion. To do this we employ $K_{ep}/K_{ee} = 3.38 \times 10^6 \text{ meV}^3$ (chosen so that $h\nu = 1.5 \text{ eV}$ conveniently corresponds to $\beta/\delta = 10^{-3}$). To match the other relevant parameters associated with the Au and Ag data in Fig. 1, we carry out calculations for $T_p = 300 \text{ K}$ over a range of photon energies $0.9 \text{ eV} \lesssim h\nu \lesssim 5.0 \text{ eV}$.⁸ We note that because T_p is fixed and $h\nu$ varies, the normalized temperature $\gamma = T_p/h\nu$ varies with the normalized ratio $\beta/\delta = K_{ep}/[K_{ee}(h\nu)^3]$. As above, we discuss our results in terms of these normalized quantities.

⁶ In reality, the average energy per excitation only asymptotically approaches that of a FD distribution. However, in the approximate theory that Gusev and Wright develop there is a point in time when such equality does occur.

⁷ See also Fig. S2 in [51].

⁸ These calculations exclude the one outlying experiment in Fig. 1, carried out at $h\nu = 0.42 \text{ eV}$.

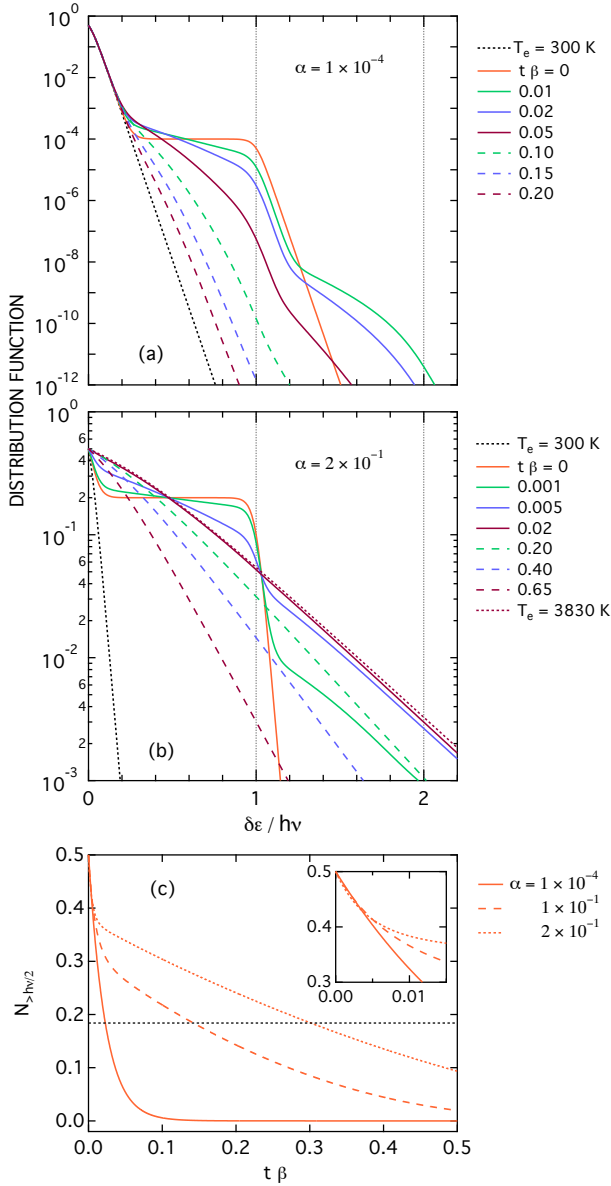


FIG. 10. Dependence of hot-carrier relaxation on normalized excitation level α in idealized Ag/Au. Panels (a) and (b) plot sequences of the distribution function $f(\delta\epsilon, t)$ at low and high excitation levels, respectively. In panel (b) the curve labeled $T_e = 3830$ K is a FD distribution at the initial (maximum) temperature in the limit of the 2T model. Panel (c) plots the time dependence of $N_{>h\nu/2}$ for three values of α . (Here $N_{>h\nu/2}$ is normalized to an initial value of $1/2$, which is the fraction of initially excited carriers with energy $\delta\epsilon > h\nu/2$.) Calculations are for $\beta/\delta = 4 \times 10^{-3}$, which corresponds to the data in Fig. 9(c).

In Fig. 9 we display results for τ_E , τ_E^{th} , τ_{th} and τ_H (all normalized by β) as functions of α for three different values of β/δ .⁹ As the figure shows, the variation of each

individual relaxation time with α is similar at all three values of β/δ . The following discussion shows that these variations are all directly related to the temperature T_e of a thermalized distribution with energy close to that of the nascent distribution.

The decrease in τ_{th} vs α is due to the increase in T_e of the target FD distribution. Associated with larger T_e values is an increase in the FD distribution $f_{FD}(\delta\epsilon, T_e)$ across the initial region of laser excitation. Therefore, fewer scattering events are required before the relaxing distribution mimics a thermal one. Additionally, these thermalizing scattering events occur (on average) more rapidly, owing to the electron-electron scattering rate τ_{ee} being proportional to $(\delta\epsilon)^{-2}$ [see Eq. (22)]. The following discussion shows this decrease of τ_{th} vs α is consequential to the behavior of both τ_E and τ_H vs α .

With regard to energy decay, recall the discussion of Fig. 7 in Sec. IV A 2. There we observe if the ratio of τ_{th} to τ_E is small enough, then intracARRIER thermalization effectively precedes energy decay and the 2T model is approximately valid. At the largest values of α in Fig. 9 this ratio indeed becomes small enough, as reflected in the fact that at the largest values of α the time constants τ_E and τ_E^{th} coalesce.

To gain insight into the dramatic upswing in τ_H at higher values of α , we plot in Fig. 10 sequences of the distribution function $f(\delta\epsilon, t)$ at both low [panel (a)] and high [panel (b)] levels of excitation. As discussed in Sec. IV A 1, the main consequence of ee scattering is to scatter the highest energy electrons to lower energy states. However, both panels (a) and (b) also show the ee interaction scatters some carriers to states with energy $\delta\epsilon/h\nu > 1$. At low excitation the number of these higher-energy carriers is negligible, as reflected in the positive change in $f(\delta\epsilon, t)$ in this region being $\lesssim 10^{-8}$. Conversely, in the high-excitation case the number of higher energy carriers is non-negligible. Furthermore, because the distribution thermalizes very quickly (notice by the time $t\beta = 0.02$ the distribution is nearly equal to a FD distribution with $T_e = 3830$ K, the maximum electron temperature in the 2T-model limit), the subsequent decay of $N_{>h\nu/2}$ (the measure for τ_H) becomes governed by energy transfer to the phonons, which is characterized by the much longer time τ_E . This behavior is readily observed in panel (c) of Fig. (10), where we plot $N_{>h\nu/2}$ for three (one low and two high) levels of excitation. The initial ($t\beta \lesssim 0.005$) decay of $N_{>h\nu/2}$ is essentially identical in all three cases (see the inset in the figure), but at the two higher levels of excitation the rapid intracARRIER thermalization at large T_e results in dramatically slower decay of $N_{>h\nu/2}$ at longer times.

The interrelated behaviors of τ_{th} and τ_E in Fig. 9 suggest three distinct regions of carrier dynamics: (i) a low

⁹ Analogous to the other relaxation times, the thermalized distri-

bution energy relaxation time τ_E^{th} is defined as the $1/e$ decay time for energy relaxation by a FD distribution.

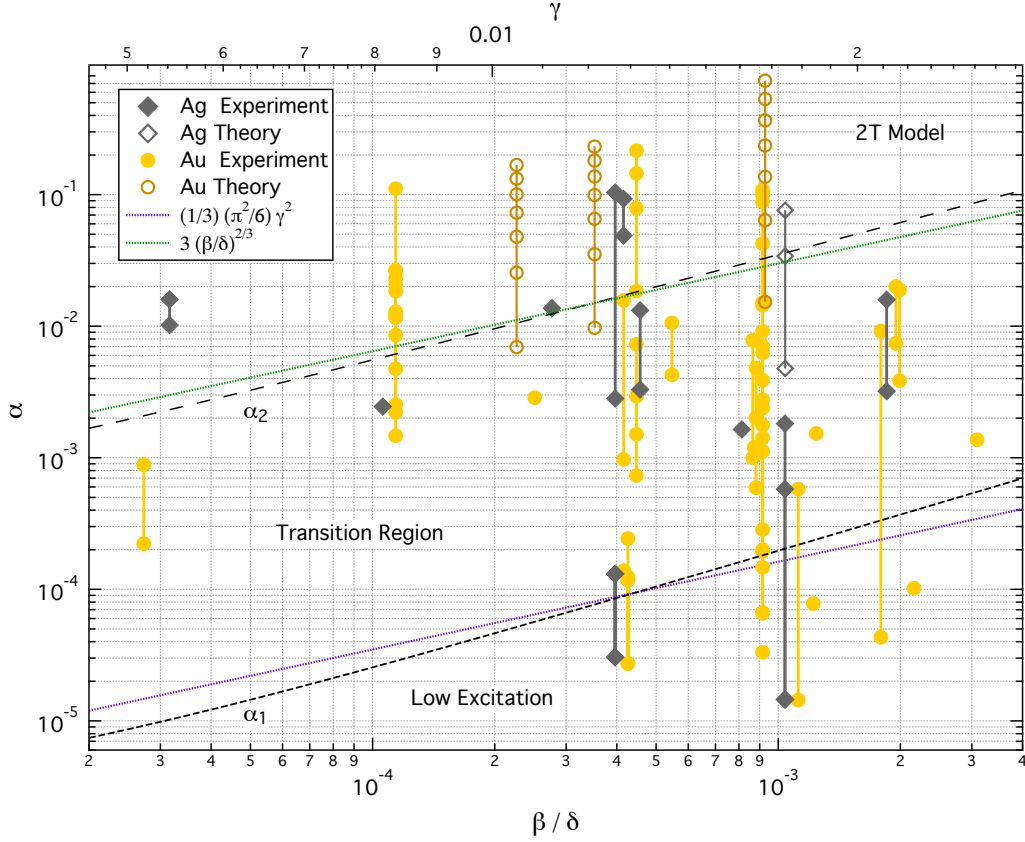


FIG. 11. Three regions of carrier relaxation behavior (shown here for Ag and Au). In the low excitation region (below the short-dashed line labeled α_1) the relaxation dynamics are independent of the excitation level α . At the highest levels of excitation (above the long-dashed line labeled α_2) the 2T model of relaxation is appropriate. In the intermediate transition region the dynamics depend upon the extent of laser excitation. (See the text for precise definitions of the α_1 and α_2 boundaries.) The values of γ indicated on the top axis correspond to RT (which applies to all of the experimental data). The experimental data are the same as those shown in Fig. 1 for Ag and Au (modulo the Au data near $\beta/\delta = 5 \times 10^{-2}$). The theoretical data are from Refs. [47] (Ag) and [48, 110] (Au). The two dotted lines are approximate α_1 and α_2 boundaries defined by Eqs. (49) and (53), respectively.

excitation region independent of the level of excitation, (ii) a transition region, and (iii) a high excitation region where the 2T model is approximately valid. To quantitatively delineate these three regions we define two boundaries. The boundary between the low excitation and transition regions we designate α_1 , which we define via

$$\tau_{th}(\alpha_1) = 0.95 \tau_{th}(\alpha \rightarrow 0). \quad (44)$$

That is, this boundary is defined as the value of α where the thermalization time τ_{th} has decreased to 95% of its value at vanishingly small α . The second boundary is designated by α_2 , which we define by the condition

$$\tau_{th}(\alpha_2) = 0.02 \tau_E(\alpha_2). \quad (45)$$

That is, α_2 is the value of α where τ_{th} equals 2% of τ_E . This choice of 2% is guided by our prior analysis of Fig. 7, where we observed that a ratio of 1.7% is sufficiently small to ensure that thermalization occurs before

significant energy decay (insofar that only $\sim 10\%$ of the excess energy in the carriers is lost to the phonons by the time the energy decay matches that of a thermal distribution). In each panel of Fig. 9 both α_1 and α_2 are indicated.

The identification of these three regions is significant with regard to ultrafast experimental studies of simple metals. In Fig. 11 we reproduce the Ag and Au data from Fig. 1. Also indicated are the two boundaries α_1 and α_2 (and thence the three regions of dynamical behavior). As is evident, these regions have significant dependence on the normalized ratio of ep to ee scattering β/δ . Clearly, a majority of the Ag and Au studies take place in the transition region between low and high excitation.

In passing, we note our numerical identification of an α independent region at low excitation levels justifies the previous BTE scattering-integral linearizations of Gusev and Wright [41], Kabanov *et al.* [43, 44], and Wilson and Coh [42].

There have been several other BTE based investiga-

tions of carrier relaxation as a function of excitation level. Tas and Maris [45] consider ee scattering only and thence propose a simple relation for τ_{th} . Expressed in our notation, their relation is

$$\tau_{th}^{TM} \delta = \frac{4}{3} \frac{1}{\alpha}. \quad (46)$$

While this relation correctly predicts that τ_{th} decreases vs α , it does not capture the transitional behavior of τ_{th} displayed by the curves in Fig. 9, which consists of a near independence from α at low excitation changing over to a strong decrease with α at high excitation. At higher values of excitation, τ_{th} does decrease with behavior that is not too different from $1/\alpha$. However, in this region of excitation the relaxation time predicted by Eq. (46) is approximately an order of magnitude too large. This can be seen in Fig. 9 by comparing our calculated values of τ_{th} with the dotted curves, which are equal to one tenth of τ_{th}^{TM} .

Other BTE based studies of excitation dependent relaxation focus on numerical results. Rethfeld *et al.* study Al [46], and Mueller and Rethfeld investigate Al and Au [48]. Both studies show the rate of thermalization has a strong dependence upon the absorbed energy density u_a . However, their calculated rates for Au are not directly comparable to our calculations in Fig. 9, owing to (i) entropy being the basis for their thermalization measure and (ii) the neglect of ep scattering in those calculations [48].

Furthermore, the parameter space investigated by these two studies is rather limited. In terms of our notation, the parameters of the Rethfeld *et al.* [46] study of Al encompass a single value of β/δ ($= 1.05 \times 10^{-3}$) and an order-of-magnitude range of α ($4.5 \times 10^{-3} \leq \alpha \leq 5.1 \times 10^{-2}$). In the Mueller and Rethfeld study [48] these parameters are $\beta/\delta = 2.16 \times 10^{-3}$ and $2.4 \times 10^{-2} \leq \alpha \leq 0.98$ for Al and $\beta/\delta = 9.3 \times 10^{-4}$ and $1.5 \times 10^{-2} \leq \alpha \leq 0.73$ for Au. In a slightly later paper Mueller and Rethfeld expand their investigation of Au to two other values of β/δ (2.3×10^{-4} and 3.5×10^{-2}) [110]. That study, however, does not report carrier relaxation times. The locations in $\beta/\delta - \alpha$ parameter space of the Mueller and Rethfeld calculations for Au [48, 110] are shown in Fig. 11 (as the open circles).¹⁰ As those data show, most of their analysis resides in the high excitation region where the 2T model is applicable.

A study of Ag by Pietanza *et al.* [47] investigates energy decay, but also at limited parameter values: $\beta/\delta = 1.03 \times 10^{-3}$ and $\alpha = 4.8 \times 10^{-3}$, 3.46×10^{-2} , and 7.6×10^{-2} . In Fig. 11 we also indicate (via open diamonds) these values. Their three sets of energy-decay

curves (see Fig. 9 of [47]) align with our analysis: (i) at the lowest level of excitation (which is within the transition region of Fig. 11), energy decay of their laser-excited distribution is significantly slower than that of the corresponding FD distribution; (ii) at the intermediate level of excitation (which nearly resides on the α_2 border), energy decay of their laser excited distribution is only slightly slower than the corresponding FD distribution; and (iii) at the highest level of excitation (which is well within the 2T-model region), their two energy decay curves are indistinguishable. Pietanza *et al.*, however, do not report energy relaxation times associated with their calculations.

We finish our discussion by developing approximate expressions for the boundaries α_1 and α_2 . For the lower boundary α_1 we begin by considering the 2T-model expression that relates the absorbed energy density u_a to the peak electron temperature $T_e^{(p)}$ and phonon temperature T_p [111],

$$\frac{u_a}{g_v} = \frac{\pi^2}{6} [(k_B T_e^{(p)})^2 - (k_B T_p)^2]. \quad (47)$$

Using Eqs. (12) and (15) this equation is readily rewritten in terms of normalized variables as

$$\frac{\alpha}{\gamma^2} = \frac{\pi^2}{6} [(\gamma_e^{(p)}/\gamma)^2 - 1]. \quad (48)$$

Even though the 2T model is not generally valid at small excitation levels, this equation suggests the low excitation region can be roughly defined by $\alpha_1/\gamma^2 = c_1 \pi^2/6$, where c_1 is some small factor. By comparing this equation with our numerical results we find

$$\alpha_1 \approx \frac{1}{3} \frac{\pi^2}{6} \gamma^2 \quad (49)$$

gives a decent description of our numerical boundary. This approximate boundary is illustrated in Fig. 11 as the dotted violet line. We note $c_1 = 1/3$ is equivalent to $\gamma_e^{(p)}/\gamma = 1.15$. Therefore, the low-excitation region roughly corresponds to the excited carriers having an effective temperature no greater than 15% of their pre-excitation temperature.

The upper boundary α_2 is defined Eq. (45). To approximate this relation we derive simple expressions for τ_{th} and τ_E at high levels of excitation. For τ_{th} we simply employ $\tau_{th}^{TM}/10$, which yields values not too far from our numerical results (see Fig. 9). We thus have [see Eq. (46)]

$$\tau_{th} \approx \frac{2}{15} \frac{1}{\alpha \delta}. \quad (50)$$

For τ_E we first note for excitations near the α_2 boundary that $\tau_E \approx \tau_E^{th}$. Hence, Eq. (23) is reasonably accurate in this excitation regime. Furthermore, because $T_e \gg T_p$ for these excitation levels we can write

$$\tau_E \approx \frac{\pi^2}{6} \frac{k_B T_e^{(p)}}{K_{ep}} = \frac{\pi^2}{6} \frac{\gamma_e^{(p)}}{\beta}. \quad (51)$$

¹⁰ Although Mueller and Rethfeld ignore ep scattering in their thermalization calculations (which is equivalent to $\beta/\delta = 0$) [48], they do include it in calculations of excitation-dependent ep coupling [48, 110].

From Eq. (48) we have $\alpha = (\pi^2/6)(\gamma_e^{(p)})^2$ at high excitation levels. We can thus express τ_E in terms of α and β as

$$\tau_E \approx \frac{\pi}{\beta} \sqrt{\frac{\alpha}{6}}. \quad (52)$$

Our approximate condition for α_2 is obtained by setting the ratio between Eqs. (50) and (52) to 0.02 [see Eq. (45)], which yields

$$\alpha_2 \approx \left(\frac{20\sqrt{6}\beta}{3\pi\delta} \right)^{2/3} \approx 3 \left(\frac{\beta}{\delta} \right)^{2/3} \quad (53)$$

This approximate boundary is illustrated in Fig. 11 as the green dotted line, which shows that for most relevant values of β/δ this simple expression is quite accurate.

V. SUMMARY

In this paper we accomplish a number of key objectives for understanding ultrafast carrier dynamics in laser excited metals. Here we review these accomplishments, which systematically extend previous general considerations of these dynamics using the Boltzmann transport equation [39–48].

(i) We employ an energy normalization of the BTE that streamlines investigation of relaxation times associated with laser-pulse-excited electron distributions. Arising from this normalization are three unitless parameters: the ep to ee scattering-strength ratio β/δ [see Eqs. (16)], excitation level α [see Eq. (12)], and phonon temperature γ [see Eq. (15)]. We assume laser excitation is instantaneous, after which the nascent distribution relaxes to an equilibrium FD distribution. From this approximation of decoupled excitation and relaxation it follows that any timescale multiplied by either β or γ is necessarily a function of only β/δ , α , and γ . This normalization allows our results to be readily applied to any simple metal.

(ii) It is important to distinguish single-carrier scattering times from relaxation times associated with an excited carrier distribution. To this end we discuss expressions for the single-carrier spontaneous phonon-emission time τ_{ep}^0 [see Eqs. (17) and (18)], total ep scattering time τ_{ep} [Eqs. (19) and (20)], and ee scattering time $\tau_{ee}(\delta\epsilon)$ [Eq. (9)]. The energy relaxation time τ_E^{th} [Eqs. (20) and (21)] for a hot thermalized distribution is also discussed. Values for all four of these times are presented in Table I and Fig. 2 for a representative selection of simple metals.

(iii) Utilizing our BTE scattering integrals [see Eqs. (2), (3), and (4)] we thoroughly investigate the behavior of three essential distribution relaxation times—hot carrier (τ_H), energy (τ_E), and thermalization (τ_{th})—as functions of β/δ at low excitation level [$\alpha = 10^{-5}$] and three different normalized phonon temperatures γ . In Fig. 4 we report six sets of time dependent distribution functions. From these (and other) distribution functions we extract values for these three relaxation times. We are

able to describe all three relaxation times using heuristic functions of β/δ [see Eqs. (31), (36), and (40)/(41)]. Because τ_H is nearly described by Matthiessen’s rule [see Eq. (31)], these two interactions act nearly independently as far as hot-carrier relaxation is concerned. A nontrivial intertwining of the two scattering mechanisms is reflected in the more complicated expressions for τ_E and τ_{th} [Eqs. (31) and (40)/(41)]. With regard to the phonon temperature, we find (i) τ_H is nearly insensitive to γ , (ii) changes in τ_E are loosely allied with $\tau_E^{th} \propto \gamma$ [see Eq. (33)], and (iii) $\tau_{th} \propto 1/\gamma^{1.8}$ when ee scattering is dominant.

(iv) These general low-excitation results are relevant to the metals listed in Table I. The two heaviest alkali metals (Rb and Cs), which are characterized by the smallest values of β/δ (typically $10^{-6} \lesssim \beta/\delta \lesssim 10^{-5}$), exhibit the simplest dynamical behavior. For these metals ee scattering is so strong (relative to ep scattering) that it controls both τ_H and τ_{th} [see Figs. 5 and 6]. Because $\tau_{th} \lesssim 0.02 \tau_E$ for these metals, thermalization occurs before significant energy transfer to the phonons. Consequently, the two-temperature (2T) model of ep dynamics [49] is a reasonable approximation. The other metals listed in Table I (excluding K and Na) are characterized by significantly larger values of β/δ (typically $10^{-4} \lesssim \beta/\delta \lesssim 5 \times 10^{-3}$). In this regime τ_H is still dominated by ee scattering, almost to the same extent as at smaller values of β/δ [see Fig. 5]. By contrast, τ_{th} has significant contribution from ep scattering. In addition, because ee scattering is relative weaker, secondary-electron generation is relatively slower; energy relaxation is consequently slower [see Fig. 6]. Lastly, in this β/δ regime τ_{th} and τ_E are similar enough that the processes of thermalization and energy relaxation happen on comparable timescales, with the end result that by the time the distribution has thermalized most of the excitation energy has transferred to the phonons (see Fig. 7). Therefore, for these metals the 2T model is a very poor approximation at low levels of excitation.

(v) We investigate the three distribution relaxation times vs excitation level α in the range $3 \times 10^{-6} \leq \alpha \leq 2 \times 10^{-1}$ (see Figs. 9, 10, and 11). The calculations are appropriate for Ag and Au at RT ($T_p = 300$ K) and photon energies $h\nu$ between 0.9 and 5 eV. The hot-carrier relaxation time τ_H is nearly invariant up to $\alpha \approx 10^{-2}$. However, in the region $10^{-2} < \alpha < 10^{-1}$ this relaxation times dramatically increases, owing to it being increasingly governed by energy relaxation, which is characterized by τ_E . Both τ_E and τ_{th} vary significantly—although more gradually than τ_H —with increasing α . The dependencies of these two relaxation times on α allow us to identify three characteristic regions of carrier relaxation: (i) a low excitation region with very little dependence on α , (ii) an intermediate region in which τ_{th} dramatically decreases and τ_E increases, and (iii) a high-excitation region where the 2T model is approximately valid. The two boundaries—designated α_1 and α_2 —that separate these three regions are given to reasonable accuracy in terms of the normalized parameters of our model by Eqs. (49)

and (53).

Appendix A: Approximate dynamics for ep scattering only

Here we compute analytic approximations to τ_H^{ep} , τ_E^{ep} , and τ_{th}^{ep} , respectively the hot-electron, energy, and thermalization relaxation times, in the limit of purely ep scattering ($\delta = 0$), respectively. Along the way we gain insight into the evolution of $f(\epsilon, t)$ under this condition.

We begin by deriving an approximate equation that governs an excited distribution in the two regions of energy (sufficiently far from ϵ_F) where the equilibrium distribution $f_{FD}(\epsilon, T_p)$ can be treated as constant (either 1 or 0). As we see below, for our standard values of $\gamma = 0.0172$ and $\alpha = 10^{-5}$, these regions are defined by $|\delta\epsilon/h\nu| \gtrsim 0.3$. We first write the distribution function as the sum

$$f(\epsilon, t) = f_{FD}(\epsilon, T_p) + \phi(\epsilon, t), \quad (\text{A1})$$

where $\phi(\epsilon, t)$ is the deviation of $f(\epsilon, t)$ from the equilibrium distribution. If we (i) substitute this form of $f(\epsilon, t)$ into the ep collision term as given by Eq. (4), (ii) recall $f_{FD}(1 - f_{FD}) = -f'_{FD} k_B T_p$, and (iii) assume this is the only collision term in the BTE, then we straightforwardly obtain for $\phi(\epsilon, t)$ the partial differential equation

$$\begin{aligned} \frac{\partial \phi}{\partial t} = K_{ep} \left[-2f'_{FD} \phi + (1 - 2f_{FD}) \frac{\partial \phi}{\partial \epsilon} \right. \\ \left. + k_B T_p \frac{\partial^2 \phi}{\partial \epsilon^2} + \phi \frac{\partial \phi}{\partial \epsilon} \right]. \end{aligned} \quad (\text{A2})$$

For energies where f_{FD} can be taken as constant this equation readily simplifies to

$$\frac{\partial \phi}{\partial t} = \mp K_{ep} \frac{\partial \phi}{\partial \epsilon} + K_{ep} k_B T_p \frac{\partial^2 \phi}{\partial \epsilon^2}. \quad (\text{A3})$$

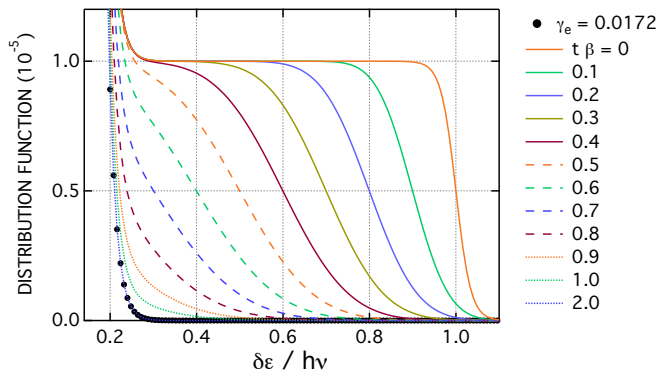


FIG. 12. Time series of distribution function $f(\delta\epsilon, t\beta)$ during relaxation for ep scattering only. Here the normalized excitation level and phonon temperature are $\alpha = 1 \times 10^{-5}$ and $\gamma = 0.0172$, respectively.

Here we have also ignored the nonlinear term in Eq. (A2), owing to it being quadratic in the (small) deviation ϕ . The minus and plus signs on the right side of this equation correspond to the regions where $\delta\epsilon$ is negative and positive, respectively.

The interpretation of Eq. (A3) is straightforward. We first note the right side comprises two terms, one convective ($\propto \partial\phi/\partial\epsilon$) and one diffusive ($\propto \partial^2\phi/\partial\epsilon^2$). If the diffusive term were absent, then the convective term would simply drive the distribution to smaller values of $|\delta\epsilon|$ at the rate K_{ep} . Physically, this convective flow arises from spontaneous phonon emission, which causes excited electrons and holes to each move towards the Fermi energy (whereupon they recombine). Conversely, if the convective term were absent, then the diffusive term would serve to increase the width of the distribution. Physically, this energy spreading arises from the sum of phonon absorption and stimulated emission.

The combination of convection and diffusion is evident in the time series of distribution functions shown in Fig. 12. We note this sequence of distributions functions are from the same set as those shown in part (b) of Fig. 3. Interestingly, pure convection is evident at the point in the distribution where $f = \alpha/2$, which is initially located at $\delta\epsilon/h\nu = 1$. Because $f = \alpha/2$ is an inflection point and $\phi(\epsilon)$ is antisymmetric about this point, the diffusive term has no effect upon this point of the distribution. Thus, the point $f = \alpha/2$ simply moves towards lower energies at the normalized rate $\beta = K_{ep}/h\nu$. As the graph shows, this behavior occurs until $t\beta \approx 0.7$, after which the effect of f_{FD} not being constant comes into play. The consequence of diffusion is also evident as the time-dependent increase in the width of the distribution's high-energy edge.

We note Gusev and Wright also consider the evolution of the distribution when ep scattering is solely at play [41]. Having derived an equation similar to Eq. (A2) [but for the whole distribution function $f(\epsilon, t)$], they state the diffusive term is only important for energies such that $\delta\epsilon \sim k_B T_p$. They then proceed to work with the equivalent of Eq. (A3), but with only the convective term. Our results displayed in Fig. 12 show such an approximation has its limitations. However, neglect of the diffusive term affords quite simple calculations of τ_H^{ep} , τ_E^{ep} , and τ_{th}^{ep} , as we now show.

To estimate these relaxation times we begin by finding an approximate solution for $\phi(\epsilon, t)$. First, we note the solution to Eq. (A3) under neglect of the diffusive term is simply

$$\phi(\delta\epsilon, 0) = \begin{cases} \phi(\delta\epsilon - K_{ep} t, 0) & \delta\epsilon < 0 \\ \phi(\delta\epsilon + K_{ep} t, 0) & \delta\epsilon > 0 \end{cases}, \quad (\text{A4})$$

Second, because $k_B T_p \ll h\nu$, the low-energy and high-energy cutoffs of $\phi(\epsilon, t)$ are rapid on the scale of $h\nu$. We thus approximate the initial distribution function as

$$\phi(\delta\epsilon, 0) = \alpha \begin{cases} -\Theta(h\nu + \delta\epsilon) & \delta\epsilon < 0 \\ \Theta(h\nu - \delta\epsilon) & \delta\epsilon > 0 \end{cases}, \quad (\text{A5})$$

where Θ is the Heaviside function. With this initial condition we immediately have

$$\phi(\delta\epsilon, t) = \alpha \begin{cases} -\Theta(h\nu - K_{ep}t + \delta\epsilon) & \delta\epsilon < 0 \\ \Theta(h\nu - K_{ep}t - \delta\epsilon) & \delta\epsilon > 0 \end{cases}. \quad (\text{A6})$$

As mentioned above, this analytic approximation for $\phi(\delta\epsilon, t)$ is valid whenever $f_{FD}(\epsilon, T_p)$ can be treated as 0 ($\delta\epsilon > 0$) or 1 ($\delta\epsilon < 0$). However, in our discussion below we shall – whenever convenient – assume Eq. (A6) is valid for all values of $\delta\epsilon$. This assumption is strictly only valid if T_p for the underlying FD distribution is zero. However, it leads to reasonably accurate results as long as $\gamma = k_B T_p / h\nu \ll 1$.

As defined in Sec. IV A 2, the hot-carrier relaxation time is the time it takes the number of excited electrons with energy above $\delta\epsilon/h\nu = 0.5$ to decay to $1/e$ of its initial value. With the approximations at hand this electron number can be written as

$$\begin{aligned} N_{>h\nu/2}(t) &= \alpha g_0 \int_{h\nu/2}^{h\nu - K_{ep}t} d(\delta\epsilon) \\ &= \alpha g_0 (h\nu/2 - K_{ep}t). \end{aligned} \quad (\text{A7})$$

From this equation it follows the hot-electron relaxation time is given by

$$\tau_H^{ep} \beta = \frac{1}{2} (1 - 1/e) = 0.3161. \quad (\text{A8})$$

As also defined in Sec. IV A 2, the energy relaxation time is the time it takes the energy in the excited distribution to fall to $1/e$ of its initial value. Given Eq. (A6), the excess energy in the excited carrier distribution is given by

$$\begin{aligned} \langle \epsilon \rangle_L(t) &= 2\alpha g_0 \int_0^{h\nu - K_{ep}t} d(\delta\epsilon) \delta\epsilon \\ &= \alpha g_0 (h\nu - K_{ep}t)^2. \end{aligned} \quad (\text{A9})$$

This expression decreases to $1/e$ of its initial value at the time τ_E^{ep} given by

$$\tau_E^{ep} \beta = 1 - 1/\sqrt{e} = 0.3935. \quad (\text{A10})$$

In Sec. IV A 2 we see that these analytic estimations for τ_H^{ep} and τ_E^{ep} are perhaps more accurate than one might have anticipated. This high degree of accuracy can be understood by considering the set of distribution functions displayed in Fig. 12. The simplicity of the results resides in the fact that over the energy range of consequence ($\delta\epsilon/h\nu \geq 0.3$) the effect of diffusion is anti-symmetric about the purely convective point $f = \alpha/2$. As far as $\tau_H^{ep} \beta \approx 0.32$ is concerned, we see up that to $t\beta = 0.3$ the lower diffusive tail extends only slightly below $\delta\epsilon/h\nu = 0.5$. Consequently, diffusion does not dramatically affect the number of hot carriers for $t < \tau_H$. Concerning $\tau_E^{ep} \beta \approx 0.39$, we see that up to $t\beta = 0.4$

the effects of diffusion only extend down to $\delta\epsilon/h\nu \approx 0.3$, while below this energy the distribution has yet to evolve. Therefore, the diffusive term also has very little effect upon the energy remaining in the carriers for $t < \tau_E$.

We now analytically approximate the thermalization time τ_{th}^{ep} . As also defined in Sec. IV A 2, τ_{th} is the time it takes the difference in $d\langle\epsilon\rangle/dt$ between the laser-excited distribution and an energy-equivalent FD distribution to decrease to $1/e$ of its initial value. For the laser-excited distribution we calculate $d\langle\epsilon\rangle/dt$ starting with $\langle\epsilon\rangle_L$ given by Eq. (A9), which yields

$$\frac{d\langle\epsilon\rangle_L}{dt} = -2K_{ep}\alpha g_0 (h\nu - K_{ep}t). \quad (\text{A11})$$

The equivalent expression for a FD distribution is given by Eq. (6). Because we want to compare laser-excited and FD distributions with identical energy, we now express T_e in terms of $\langle\epsilon\rangle_L$. Equating this energy with that of a FD distribution [111]

$$\langle\epsilon\rangle_{FD} = \frac{\pi^2}{6} g_0 k_B^2 (T_e^2 - T_p^2). \quad (\text{A12})$$

we find

$$k_B^2 T_e^2 = \frac{6}{\pi^2} \frac{\langle\epsilon\rangle_L}{g_0} + k_B^2 T_p^2, \quad (\text{A13})$$

which allows us to rewrite Eq. (6) as

$$\frac{d\langle\epsilon\rangle_{FD}}{dt} = -K_{ep}g_0 \left[\sqrt{\frac{6}{\pi^2} \frac{\langle\epsilon\rangle_L}{g_0} + k_B^2 T_p^2} - k_B T_p \right]. \quad (\text{A14})$$

Our present interest is the limit of low excitation, in which case Eq. (A14) simplifies to

$$\begin{aligned} \frac{d\langle\epsilon\rangle_{FD}}{dt} &= -\frac{3}{\pi^2} K_{ep} \frac{\langle\epsilon\rangle_L}{k_B T_p} \\ &= -\frac{3}{\pi^2} K_{ep} \alpha g_0 \frac{(h\nu - K_{ep}t)^2}{k_B T_p}. \end{aligned} \quad (\text{A15})$$

Taking the difference between $d\langle\epsilon\rangle_{FD}/dt$ and $d\langle\epsilon\rangle_L/dt$ as given by Eqs. (A15) and (A11) we find τ_{th}^{ep} is determined by the quadratic equation

$$\frac{3}{\pi^2} \frac{1}{\gamma} (1 - \tau_{th}^{ep} \beta)^2 - 2(1 - \tau_{th}^{ep} \beta) = \frac{1}{e} \left(\frac{3}{\pi^2} \frac{1}{\gamma} - 2 \right). \quad (\text{A16})$$

We note for our conditions of interest the term quadratic in $(1 - \tau_{th}^{ep} \beta)$ is significantly larger than the linear term. Therefore, $\tau_{th}^{ep} \beta$ is close to $\tau_E^{ep} \beta$ [which is solely controlled by this same quadratic term, see Eq. (A9)]. Indeed, for $\gamma = 0.0086, 0.0172$, and 0.0344 , the solutions to Eq. (A16) are $\tau_{th}^{ep} \beta = 0.3819, 0.3694$, and 0.3415 , respectively, which are not far from the analytic result 0.3935 for $\tau_E^{ep} \beta$ [see Eq. (A10)]. These analytic values for $\tau_{th}^{ep} \beta$ are also reasonably close to the corresponding numerically calculated values $0.3944, 0.3848$, and 0.3766 [see Table II].

- [1] M. Battiato, K. Carva, and P. M. Oppeneer, "Superdiffusive spin transport as a mechanism of ultrafast demagnetization," *Physical Review Letters* **105**, 027203 (2010).
- [2] A. J. Schellekens, K. C. Kuiper, R. R. J. C. De Wit, and B. Koopmans, "Ultrafast spin-transfer torque driven by femtosecond pulsed-laser excitation," *Nature Communications* **5**, 4333 (2014).
- [3] G.-M. Choi, C.-H. Moon, B.-C. Min, K.-J. Lee, and D. G. Cahill, "Thermal spin-transfer torque driven by the spin-dependent Seebeck effect in metallic spin-valves," *Nature Physics* **11**, 576–581 (2015).
- [4] R. B. Wilson, Y. Yang, J. Gorchon, C.-H. Lambert, S. Salahuddin, and J. Bokor, "Electric current induced ultrafast demagnetization," *Phys. Rev. B* **96**, 045105 (2017).
- [5] R. B. Wilson, J. Gorchon, Y. Yang, C.-H. Lambert, S. Salahuddin, and J. Bokor, "Ultrafast magnetic switching of GdFeCo with electronic heat currents," *Phys. Rev. B* **95**, 180409(R) (2017).
- [6] Y. Yang, R. B. Wilson, J. Gorchon, C.-H. Lambert, S. Salahuddin, and J. Bokor, "Ultrafast magnetization reversal by picosecond electrical pulses," *Science Advances* **3**, e1603117 (2017).
- [7] A. Alekhin, I. Razdolski, N. Ilin, J. P. Meyburg, D. Diesing, V. Roddatis, I. Rungger, M. Stamenova, S. Sanvito, U. Bovensiepen, and A. Melnikov, "Femtosecond spin current pulses generated by the nonthermal spin-dependent Seebeck effect and interacting with ferromagnets in spin valves," *Phys. Rev. Lett.* **119**, 017202 (2017).
- [8] T. S. Seifert, S. Jaiswal, J. Barker, S. T. Weber, I. Razdolski, J. Cramer, O. Gueckstock, S. F. Maehrlein, L. Nadvornik, S. Watanabe, *et al.*, "Femtosecond formation dynamics of the spin Seebeck effect revealed by terahertz spectroscopy," *Nature Communications* **9**, 2899 (2018).
- [9] S. Linic, U. Aslam, C. Boerigter, and M. Morabito, "Photochemical transformations on plasmonic metal nanoparticles," *Nature Materials* **14**, 567–576 (2015).
- [10] Y. Zhang, S. He, W. Guo, Y. Hu, J. Huang, J. R. Mulcahy, and W. D. Wei, "Surface-plasmon-driven hot electron photochemistry," *Chemical Reviews* **118**, 2927–2954 (2018).
- [11] U. Aslam, V. G. Rao, S. Chavez, and S. Linic, "Catalytic conversion of solar to chemical energy on plasmonic metal nanostructures," *Nature Catalysis* **1**, 656–665 (2018).
- [12] J. Szczerbiński, L. Gyr, J. Kaeslin, and R. Zenobi, "Plasmon-driven photocatalysis leads to products known from e-beam and X-ray-induced surface chemistry," *Nano Letters* **18**, 6740–6749 (2018).
- [13] C. Clavero, "Plasmon-induced hot-electron generation at nanoparticle/metal-oxide interfaces for photovoltaic and photocatalytic devices," *Nature Photonics* **8**, 95–103 (2014).
- [14] K. Wu, J. Chen, J. R. McBride, and T. Lian, "Efficient hot-electron transfer by a plasmon-induced interfacial charge-transfer transition," *Science* **349**, 632–635 (2015).
- [15] Y. H. Jang, Y. J. Jang, S. Kim, L. N. Quan, K. Chung, and D. H. Kim, "Plasmonic solar cells: From rational design to mechanism overview," *Chemical Reviews* **116**, 14982–15034 (2016).
- [16] J. Chen, W.-K. Chen, J. Tang, and P. M. Rentzepis, "Time-resolved structural dynamics of thin metal films heated with femtosecond optical pulses," *Proceedings of the National Academy of Sciences* **108**, 18887–18892 (2011).
- [17] J. Chen, W.-K. Chen, and P. M. Rentzepis, "Blast wave and contraction in Au(111) thin film induced by femtosecond laser pulses. A time resolved x-ray diffraction study," *Journal of Applied Physics* **109**, 113522 (2011).
- [18] T. G. White, P. Mabey, D. O. Gericke, N. J. Hartley, H. W. Doyle, D. McGonegle, D. S. Rackstraw, A. Higginbotham, and G. Gregori, "Electron-phonon equilibration in laser-heated gold films," *Phys. Rev. B* **90**, 014305 (2014).
- [19] W. Lu, M. Nicoul, U. Shymanovich, F. Brinks, M. Afshari, A. Tarasevitch, D. von der Linde, and K. Sokolowski-Tinten, "Acoustic response of a laser-excited polycrystalline Au-film studied by ultrafast Debye-Scherrer diffraction at a table-top short-pulse x-ray source," *AIP Advances* **10**, 035015 (2020).
- [20] H. Park, X. Wang, S. Nie, R. Clinite, and J. Cao, "Mechanism of coherent acoustic phonon generation under nonequilibrium conditions," *Phys. Rev. B* **72**, 100301(R) (2005).
- [21] S. Nie, X. Wang, H. Park, R. Clinite, and J. Cao, "Measurement of the electronic Grüneisen constant using femtosecond electron diffraction," *Phys. Rev. Lett.* **96**, 025901 (2006).
- [22] M. Ligges, I. Rajkovic, P. Zhou, O. Posth, C. Hassel, G. Dumpich, and D. von der Linde, "Observation of ultrafast lattice heating using time resolved electron diffraction," *Applied Physics Letters* **94**, 101910 (2009).
- [23] M. Ligges, I. Rajković, C. Streubühr, T. Brazda, P. Zhou, O. Posth, C. Hassel, G. Dumpich, and D. von der Linde, "Transient (000)-order attenuation effects in ultrafast transmission electron diffraction," *Journal of Applied Physics* **109**, 065519 (2011).
- [24] T. Chase, M. Trigo, A. H. Reid, R. Li, T. Vecchione, X. Shen, S. Weathersby, R. Coffee, N. Hartmann, D. A. Reis, X. J. Wang, and H. A. Dürr, "Ultrafast electron diffraction from non-equilibrium phonons in femtosecond laser heated Au films," *Applied Physics Letters* **108**, 041909 (2016).
- [25] K. Sokolowski-Tinten, X. Shen, Q. Zheng, T. Chase, R. Coffee, M. Jerman, M. Li, R. K. and Ligges, I. Makasyuk, M. Mo, A. H. Reid, B. Rethfeld, T. Vecchione, S. P. Weathersby, H. A. Dürr, and X. J. Wang, "Electron-lattice energy relaxation in laser-excited thin-film Au-insulator heterostructures studied by ultrafast MeV electron diffraction," *Structural Dynamics* **4**, 054501 (2017).
- [26] M. Z. Mo, V. Becker, B. K. Ofori-Okai, X. Shen, Z. Chen, B. Witte, R. Redmer, R. K. Li, M. Dunning, S. P. Weathersby, X. J. Wang, and S. H. Glenzer, "Determination of the electron-lattice coupling strength of copper with ultrafast MeV electron diffraction," *Review*

- of *Scientific Instruments* **89**, 10C108 (2018).
- [27] A. Carattino, M. Caldarola, and M. Orrit, “Gold nanoparticles as absolute nanothermometers,” *Nano Letters* **18**, 874–880 (2018).
- [28] T. Jollans, M. Caldarola, Y. Sivan, and M. Orrit, “Effective electron temperature measurement using time-resolved anti-Stokes photoluminescence,” *The Journal of Physical Chemistry A* **124**, 6968–6976 (2020).
- [29] N. Hogan, S. Wu, and M. Sheldon, “Photothermalization and hot electron dynamics in the steady state,” *The Journal of Physical Chemistry C* **124**, 4931–4945 (2020).
- [30] S. Wu, Oscar H.-C. Cheng, B. Zhao, N. Hogan, A. Lee, D. H. Son, and M. Sheldon, “The connection between plasmon decay dynamics and the surface enhanced Raman spectroscopy background: Inelastic scattering from non-thermal and hot carriers,” *Journal of Applied Physics* **129**, 173103 (2021).
- [31] J. Huang, W. Wang, C. J. Murphy, and D. G. Cahill, “Resonant secondary light emission from plasmonic Au nanostructures at high electron temperatures created by pulsed-laser excitation,” *Proceedings of the National Academy of Sciences* **111**, 906–911 (2014).
- [32] Y.-Y. Cai, E. Sung, R. Zhang, L. J. Tauzin, J. G. Liu, B. Ostovar, Y. Zhang, W.-S. Chang, P. Nordlander, and S. Link, “Anti-Stokes emission from hot carriers in gold nanorods,” *Nano Letters* **19**, 1067–1073 (2019).
- [33] T. Suemoto, K. I. Yamanaka, and N. Sugimoto, “Observation of femtosecond infrared luminescence in gold,” *Phys. Rev. B* **100**, 125405 (2019).
- [34] S. Ono and T. Suemoto, “Ultrafast photoluminescence in metals: Theory and its application to silver,” *Phys. Rev. B* **102**, 024308 (2020).
- [35] T. Suemoto, K. Yamanaka, N. Sugimoto, T. Otsu, S. Tani, Y. Kobayashi, and T. Koyama, “Effect of emissivity on ultrafast luminescence spectra in silver,” *Journal of Applied Physics* **128**, 203101 (2020).
- [36] T. Suemoto, K. Yamanaka, N. Sugimoto, Y. Kobayashi, T. Otsu, S. Tani, and T. Koyama, “Relaxation dynamics of hot electrons in the transition metals Au, Ag, Cu, Pt, Pd, and Ni studied by ultrafast luminescence spectroscopy,” *Journal of Applied Physics* **130**, 025101 (2021).
- [37] Y. Sivan, I. W. Un, I. Kalyan, K.-Q. Lin, J. M. Lupton, and S. Bange, “Crossover from nonthermal to thermal photoluminescence from metals excited by ultrashort light pulses,” *ACS Nano* **17**, 11439–11453 (2023).
- [38] Á. Rodríguez Echarri, F. Iyikanat, S. Boroviks, N. A. Mortensen, J. D. Cox, and F. J. García de Abajo, “Nonlinear photoluminescence in gold thin films,” *ACS Photonics* **10**, 2918–2929 (2023).
- [39] R. H. M. Groeneveld, R. Sprik, and A. Lagendijk, “Effect of a nonthermal electron distribution on the electron-phonon energy relaxation process in noble metals,” *Phys. Rev. B* **45**, 5079–5082 (1992).
- [40] R. H. M. Groeneveld, R. Sprik, and A. Lagendijk, “Femtosecond spectroscopy of electron-electron and electron-phonon energy relaxation in Ag and Au,” *Phys. Rev. B* **51**, 11433–11445 (1995).
- [41] V. E. Gusev and O. B. Wright, “Ultrafast nonequilibrium dynamics of electrons in metals,” *Phys. Rev. B* **57**, 2878–2888 (1998).
- [42] R. B. Wilson and S. Coh, “Parametric dependence of hot electron relaxation timescales on electron-electron and electron-phonon interaction strengths,” *Communications Physics* **3**, 179 (2020).
- [43] V. V. Kabanov and A. S. Alexandrov, “Electron relaxation in metals: Theory and exact analytical solutions,” *Phys. Rev. B* **78**, 174514 (2008).
- [44] V. V. Baranov and V. V. Kabanov, “Theory of electronic relaxation in a metal excited by an ultrashort optical pump,” *Phys. Rev. B* **89**, 125102 (2014).
- [45] G. Tas and H. J. Maris, “Electron diffusion in metals studied by picosecond ultrasonics,” *Phys. Rev. B* **49**, 15046–15054 (1994).
- [46] B. Rethfeld, A. Kaiser, M. Vicanek, and G. Simon, “Ultrafast dynamics of nonequilibrium electrons in metals under femtosecond laser irradiation,” *Phys. Rev. B* **65**, 214303 (2002).
- [47] L. D. Pietanza, G. Colonna, S. Longo, and M. Capitelli, “Non-equilibrium electron and phonon dynamics in metals under femtosecond laser pulses,” *The European Physical Journal D* **45**, 369–389 (2007).
- [48] B. Y. Mueller and B. Rethfeld, “Relaxation dynamics in laser-excited metals under nonequilibrium conditions,” *Phys. Rev. B* **87**, 035139 (2013).
- [49] S. I. Anisimov, B. L. Kapeliovich, and T. L. Perelman, “Electron emission from metal surfaces exposed to ultrashort laser pulses,” *Soviet Physics-JETP* **39**, 375–377 (1974).
- [50] D. M. Riffe and R. B. Wilson, “Excitation and relaxation of nonthermal electron energy distributions in metals with application to gold,” *Phys. Rev. B* **107**, 214309 (2023).
- [51] See Supplemental Material at [URL will be inserted by publisher] for details concerning (i) the experimental data presented in Fig. 1 and 11, (ii) least-squares analysis of our relaxation-time data, and (iii) the initial time dependence of $f(\epsilon, t)$.
- [52] H. E. Elsayed-Ali, T. B. Norris, M. A. Pessot, and G. A. Mourou, “Time-resolved observation of electron-phonon relaxation in copper,” *Phys. Rev. Lett.* **58**, 1212–1215 (1987).
- [53] J. Hohlfeld, D. Grosenick, U. Conrad, and E. Matthias, “Femtosecond time-resolved reflection second-harmonic generation on polycrystalline copper,” *Applied Physics A* **60**, 137–142 (1995).
- [54] J. Hohlfeld, U. Conrad, and E. Matthias, “Does femtosecond time-resolved second-harmonic generation probe electron temperatures at surfaces?” *Applied Physics B* **63**, 541–544 (1996).
- [55] N. A. Papadogiannis, S. D. Moustazis, and J. P. Girardeau-Montaut, “Electron relaxation phenomena on a copper surface via nonlinear ultrashort single-photon photoelectric emission,” *Journal of Physics D: Applied Physics* **30**, 2389–2396 (1997).
- [56] A. Bartoli, G. Ferrini, L. Fini, G. Gabetta, F. Parmigiani, and F. T. Arecchi, “Nonlinear photoemission from W and Cu investigated by total-yield correlation measurements,” *Phys. Rev. B* **56**, 1107–1110 (1997).
- [57] VM Farztdinov, AL Dobryakov, SA Kovalenko, DV Lisin, SP Merkulova, F Pudonin, and Yu E Lozovik, “Ultrafast phenomena in copper films,” *Physica Scripta* **60**, 579–583 (1999).
- [58] M. Bonn, D. N. Denzler, S. Funk, M. Wolf, S.-S. Wellerhoff, and J. Hohlfeld, “Ultrafast electron dynamics at

- metal surfaces: Competition between electron-phonon coupling and hot-electron transport,” *Phys. Rev. B* **61**, 1101–1105 (2000).
- [59] V. V. Kruglyak, R. J. Hicken, M. Ali, B. J. Hickey, A. T. G. Pym, and B. K. Tanner, “Measurement of hot electron momentum relaxation times in metals by femtosecond ellipsometry,” *Phys. Rev. B* **71**, 233104 (2005).
- [60] X. Shen, Y. P. Timalsina, T.-M. Lu, and M. Yamaguchi, “Experimental study of electron-phonon coupling and electron internal thermalization in epitaxially grown ultrathin copper films,” *Phys. Rev. B* **91**, 045129 (2015).
- [61] A. Nakamura, T. Shimojima, M. Nakano, Y. Iwasa, and K. Ishizaka, “Electron and lattice dynamics of transition metal thin films observed by ultrafast electron diffraction and transient optical measurements,” *Structural Dynamics* **3**, 064501 (2016).
- [62] M. Obergfell and J. Demsar, “Tracking the time evolution of the electron distribution function in copper by femtosecond broadband optical spectroscopy,” *Phys. Rev. Lett.* **124**, 037401 (2020).
- [63] D. M. Riffe, X. Y. Wang, M. Downer, D. L. Fisher, T. Tajima, J. L. Erskine, and R. M. More, “Femtosecond thermionic emission from metals in the space-charge-limited regime,” *JOSA B* **10**, 1424–1435 (1993).
- [64] N. Del Fatti, R. Bouffanais, F. Vallée, and C. Flytzanis, “Nonequilibrium electron interactions in metal films,” *Phys. Rev. Lett.* **81**, 922–925 (1998).
- [65] N. Del Fatti, C. Voisin, M. Achermann, S. Tzortzakis, D. Christofilos, and F. Vallée, “Nonequilibrium electron dynamics in noble metals,” *Phys. Rev. B* **61**, 16956–16966 (2000).
- [66] D. T. Owens, C. Fuentes-Hernandez, J. M. Hales, J. W. Perry, and B. Kippelen, “A comprehensive analysis of the contributions to the nonlinear optical properties of thin Ag films,” *Journal of Applied Physics* **107**, 123114 (2010).
- [67] A. Oguz Er, J. Chen, J. Tang, and P. M. Rentzepis, “Transient lattice distortion induced by ultrashort heat pulse propagation through thin film metal/metal interface,” *Applied Physics Letters* **102**, 051915 (2013).
- [68] R. W. Schoenlein, W. Z. Lin, J. G. Fujimoto, and G. L. Eesley, “Femtosecond studies of nonequilibrium electronic processes in metals,” *Phys. Rev. Lett.* **58**, 1680–1683 (1987).
- [69] S. D. Brorson, J. G. Fujimoto, and E. P. Ippen, “Femtosecond electronic heat-transport dynamics in thin gold films,” *Phys. Rev. Lett.* **59**, 1962–1965 (1987).
- [70] H. E. Elsayed-Ali, T. Juhasz, G. O. Smith, and W. E. Bron, “Femtosecond thermorefectivity and thermo-transmissivity of polycrystalline and single-crystalline gold films,” *Phys. Rev. B* **43**, 4488–4491 (1991).
- [71] W. S. Fann, R. Storz, H. W. K. Tom, and J. Bokor, “Electron thermalization in gold,” *Phys. Rev. B* **46**, 13592–13595 (1992).
- [72] T. Juhasz, H. E. Elsayed-Ali, X. H. Hu, and W. E. Bron, “Time-resolved thermorefectivity of thin gold films and its dependence on the ambient temperature,” *Phys. Rev. B* **45**, 13819–13822 (1992).
- [73] T. Juhasz, H. E. Elsayed-Ali, G. O. Smith, C. Suárez, and W. E. Bron, “Direct measurements of the transport of nonequilibrium electrons in gold films with different crystal structures,” *Phys. Rev. B* **48**, 15488–15491 (1993).
- [74] J. P. Girardeau-Montaut, C. Girardeau-Montaut, S. D. Moustazis, and C. Fotakis, “High current density produced by femtosecond nonlinear single-photon photoelectric emission from gold,” *Applied Physics Letters* **62**, 426–428 (1993).
- [75] C.-K. Sun, F. Vallée, L. Acioli, E. P. Ippen, and J. G. Fujimoto, “Femtosecond investigation of electron thermalization in gold,” *Phys. Rev. B* **48**, 12365–12368 (1993).
- [76] C.-K. Sun, F. Vallée, L. H. Acioli, E. P. Ippen, and J. G. Fujimoto, “Femtosecond-tunable measurement of electron thermalization in gold,” *Phys. Rev. B* **50**, 15337–15348 (1994).
- [77] X. Y. Wang, D. M. Riffe, Y.-S. Lee, and M. C. Downer, “Time-resolved electron-temperature measurement in a highly excited gold target using femtosecond thermionic emission,” *Phys. Rev. B* **50**, 8016–8019 (1994).
- [78] J. Hohlfeld, J. G. Müller, S.-Svante Wellershoff, and E. Matthias, “Time-resolved thermorefectivity of thin gold films and its dependence on film thickness,” *Applied Physics B* **64**, 387–390 (1997).
- [79] A. A. Maznev, J. Hohlfeld, and J. Güdde, “Surface thermal expansion of metal under femtosecond laser irradiation,” *Journal of Applied Physics* **82**, 5082–5085 (1997).
- [80] K. L. Moore and T. D. Donnelly, “Probing nonequilibrium electron distributions in gold by use of second-harmonic generation,” *Optics Letters* **24**, 990–992 (1999).
- [81] A. Hibara, T. Morishita, I. Tsuyumoto, A. Harata, T. Kitamori, and T. Sawada, “Direct measurements of femtosecond energy dissipation processes of hot electrons in a gold film,” *Japanese Journal of Applied Physics* **38**, 2983 (1999).
- [82] J. L. Hostetler, A. N. Smith, D. M. Czajkowsky, and P. M. Norris, “Measurement of the electron-phonon coupling factor dependence on film thickness and grain size in Au, Cr, and Al,” *Appl. Opt.* **38**, 3614–3620 (1999).
- [83] A. N. Smith, J. L. Hostetler, and P. M. Norris, “Thermal boundary resistance measurements using a transient thermorefectance technique,” *Microscale Thermophysical Engineering* **4**, 51–60 (2000).
- [84] A. N. Smith and P. M. Norris, “Influence of intraband transitions on the electron thermorefectance response of metals,” *Applied Physics Letters* **78**, 1240–1242 (2001).
- [85] C. Guo, G. Rodriguez, and A. J. Taylor, “Ultrafast dynamics of electron thermalization in gold,” *Phys. Rev. Lett.* **86**, 1638–1641 (2001).
- [86] W. M. G. Ibrahim, H. E. Elsayed-Ali, C. E. Bonner, and M. Shinn, “Ultrafast investigation of electron dynamics in multi-layer metals,” *International Journal of Heat and Mass Transfer* **47**, 2261–2268 (2004).
- [87] P. E. Hopkins and P. M. Norris, “Substrate influence in electron-phonon coupling measurements in thin Au films,” *Applied Surface Science* **253**, 6289–6294 (2007).
- [88] W. G. Ma, H. D. Wang, X. Zhang, and W. Wang, “Experiment study of the size effects on electron-phonon relaxation and electrical resistivity of polycrystalline thin gold films,” *Journal of Applied Physics* **108**, 064308 (2010).
- [89] P. E. Hopkins, L. M. Phinney, and J. R. Serrano, “Re-

- examining electron-Fermi relaxation in gold films with a nonlinear thermoreflectance model,” *Journal of Heat Transfer* **133**, 044505 (2011).
- [90] G. Della Valle, M. Conforti, S. Longhi, G. Cerullo, and D. Brida, “Real-time optical mapping of the dynamics of nonthermal electrons in thin gold films,” *Phys. Rev. B* **86**, 155139 (2012).
- [91] A. A. Kolomenskii, R. Mueller, J. Wood, J. Strohaber, and H. A. Schuessler, “Femtosecond electron-lattice thermalization dynamics in a gold film probed by pulsed surface plasmon resonance,” *Applied Optics* **52**, 7352–7359 (2013).
- [92] P. E. Hopkins, J. C. Duda, B. Kaehr, X. W. Zhou, C.-Y. P. Yang, and R. E. Jones, “Ultrafast and steady-state laser heating effects on electron relaxation and phonon coupling mechanisms in thin gold films,” *Applied Physics Letters* **103**, 211910 (2013).
- [93] Liang Guo and Xianfan Xu, “Ultrafast spectroscopy of electron-phonon coupling in gold,” *Journal of Heat Transfer* **136**, 122401 (2014).
- [94] T. Heilpern, M. Manjare, A. O. Govorov, G. P. Wiederrecht, S. K. Gray, and H. Harutyunyan, “Determination of hot carrier energy distributions from inversion of ultrafast pump-probe reflectivity measurements,” *Nature Communications* **9**, 1–6 (2018).
- [95] Q. Yao, L. Guo, V. Iyer, and X. Xu, “Ultrafast electron-phonon coupling at metal-dielectric interface,” *Heat Transfer Engineering*, 1211–1219 (2018).
- [96] H. J. Sielcken and H. J. Bakker, “Probing the ultrafast electron and lattice dynamics of gold using femtosecond mid-infrared pulses,” *Phys. Rev. B* **102**, 134301 (2020).
- [97] J. A. Tomko, S. Kumar, R. Sundararaman, and P. E. Hopkins, “Temperature dependent electron-phonon coupling of Au resolved via lattice dynamics measured with sub-picosecond infrared pulses,” *Journal of Applied Physics* **129**, 193104 (2021).
- [98] S. Grauby, B. Vidal Montes, A. Zenji, J.-M. Rampnoux, and S. Dilhaire, “How to measure hot electron and phonon temperatures with time domain thermoreflectance spectroscopy?” *ACS Photonics* **9**, 3734–3744 (2022).
- [99] R. J. Stevens, A. N. Smith, and P. M. Norris, “Measurement of thermal boundary conductance of a series of metal-dielectric interfaces by the transient thermoreflectance technique,” *J. Heat Transfer* **127**, 315–322 (2005).
- [100] W. Ma, H. Wang, X. Zhang, and W. Wang, “Study of the electron-phonon relaxation in thin metal films using transient thermoreflectance technique,” *International Journal of Thermophysics* **34**, 2400–2415 (2013).
- [101] L. Waldecker, R. Bertoni, R. Ernstorfer, and J. Vorberger, “Electron-phonon coupling and energy flow in a simple metal beyond the two-temperature approximation,” *Phys. Rev. X* **6**, 021003 (2016).
- [102] G. Grimvall, *The Electron-Phonon Interaction in Metals* (North Holland, New York, 1981).
- [103] R. B. Wilson, *An Embedded Atom Method Investigation into the Lattice Dynamics of Metallic Surfaces*, Master’s thesis, Utah State University (2011).
- [104] W. A. Kamitakahara and B. N. Brockhouse, “Crystal dynamics of silver,” *Physics Letters A* **29**, 639–640 (1969).
- [105] V. N. Antonov, V. Y. Milman, V. V. Nemoskhalenko, and A. V. Zhalko-Titarenko, “Lattice dynamics of FCC transition metals: A pseudopotential approach,” *Zeitschrift für Physik B Condensed Matter* **79**, 223–232 (1990).
- [106] P. B. Allen, “Theory of thermal relaxation of electrons in metals,” *Phys. Rev. Lett.* **59**, 1460–1463 (1987).
- [107] M. Bauer, A. Marienfeld, and M. Aeschlimann, “Hot electron lifetimes in metals probed by time-resolved two-photon photoemission,” *Progress in Surface Science* **90**, 319–376 (2015).
- [108] D. Pines and P. Nozieres, *The Theory of Quantum Liquids* (Benjamin, New York, 1966).
- [109] D. A. Papaconstantopoulos, *Handbook of the Band Structure of Elemental Solids* (Springer, New York, 1986).
- [110] B. Y. Mueller and B. Rethfeld, “Nonequilibrium electron-phonon coupling after ultrashort laser excitation of gold,” *Applied Surface Science* **302**, 24–28 (2014).
- [111] N. W. Ashcroft and N. D. Mermin, *Solid State Physics* (Saunders College Publishing, 1976).

Supplemental Material for “Ultrafast relaxation dynamics of excited carriers in metals: Simplifying the intertwined dependencies upon scattering strengths, phonon temperature, photon energy, and excitation level”

D. M. Riffe

Physics Department, Utah State University, Logan, UT 84322, USA

Richard B. Wilson

Mechanical Engineering Department and Materials Science and Engineering Department, University of California, Riverside, CA 92521, USA

SI. β/δ AND α DATA IN FIGS. 1 AND 11

In Figs. 1 and 11 of the paper we plot concurrent values of the normalized interaction strength ratio

$$\beta/\delta = \frac{K_{ep}}{K_{ee}(h\nu)^3} \quad (\text{S1})$$

and normalized excitation level

$$\alpha = \frac{u_d}{(h\nu)^2 g_v} \quad (\text{S2})$$

relevant to a wide variety experiments on Cu, Ag, Au, and Al. In each experiment the sample—a thin film or bulk sample at room temperature—is excited by sub-ps laser pulses. In most experiments several values of the incident fluence F_i are utilized, although some experiments are carried out at a single fluence. We now describe how we infer the values of β/δ and α relevant to each experiment.

Values of β/δ are straightforwardly obtained, as all experiments report the photon energy $h\nu$ utilized. With this parameter and the K_{ep} and K_{ee} values reported in Table I, β/δ is obtained from Eq. (S1).

More effort is required to deduce values of α . As Eq. (S2) indicates, we also need the electronic density of states g_v (at the Fermi level) and the energy density u_d absorbed by the sample when excited by a single laser pulse. For g_v we use values calculated by Papaconstantopolous.¹ The absorbed energy density is related to F_i (which is usually reported) via

$$u_d = \frac{F_i A}{d}, \quad (\text{S3})$$

where A is the absorptivity (fraction of incident energy absorbed) and d is the depth over which the absorbed energy is initially deposited in the sample. In most cases we calculate A using thin-film optics relations for normal-incidence radiation,² although when required we utilize Fresnel relations for non-normal incidence.³ The length d is possibly one of three quantities. If the sample is thin enough, then carrier transport that occurs during the laser pulse will ensure that the initial energy is spread fairly uniformly from the front to the back of the sample. In this case $d = d_s$, where d_s is the sample thickness. However, it may be that transport is not fast enough to enable such uniform heating. For each experiment we thus calculate the 1D diffusion length $d_D = d_m \sqrt{\Delta t (3\tau_s)^{-1}}$. Here Δt is the laser-pulse duration, τ_s is the average single-carrier scattering time, and $d_m = v_F \tau_s$ is the carrier mean free path. We take τ_s to be the scattering time (from ep and ee interactions) for an electron with energy $\delta\epsilon = h\nu/2$, which is given by $\tau_s^{-1} = (\tau_{ep}(T_p))^{-1} + (\tau_{ee}(h\nu/2))^{-1}$. A third length scale is also important, the intensity skin depth d_I of the incident radiation. If the larger of d_D and d_I is smaller than d_s , then d is taken to be that larger value. Otherwise, we assume $d = d_s$. In more mathematical notation, d is determined by

$$d = \min(d_s, \max(d_I, d_D)). \quad (\text{S4})$$

Strictly speaking, the thin-film optics relations we use to calculate the absorptivity A are only valid in the low-excitation (linear-response) limit. At high levels of excitation stimulated emission should be

included when determining the absorbed energy density. We include in approximate fashion the effect of stimulated emission by using—instead of Eq. (S2)—the relation

$$\alpha = \frac{1 - e^{-2\frac{u_d}{(h\nu)^2 g_v}}}{2}, \quad (\text{S5})$$

where u_d is still calculated via the linear-response relation Eq. (S3). Equation (S5) is derived under the assumption that excited electrons are not subsequently excited by another photon. Notice at low excitation (small values of $u_d/[(h\nu)^2 g_v]$) Eq. (S5) simplifies to Eq. (S2), but at high excitation α is limited to values less than 1/2, as expected.

In Tables S1 - S4 we list values of β/δ and the range of α values appropriate to the experiments on Cu,⁴⁻¹⁸ Ag,^{6,11,13,18-24} Au,^{6,10-13,15,18,20,22,25-60} and Al^{19,39,61-66} represented in Figs. 1 and 11.

TABLE S1. Values of β/δ and range of α values (indicated by α_{\min} and α_{\max}) in experimental investigations of room-temperature Cu excited by sub-ps laser pulses. Experiments with only α_{\min} indicated were carried out at a single excitation level.

Cu			
Study	β/δ	α_{\min}	α_{\max}
Elsayed-Ali (1987) [4]	6.55×10^{-4}	4.75×10^{-3}	3.73×10^{-2}
Hohlfeld (1995) [5]	6.71×10^{-4}	6.52×10^{-2}	1.22×10^{-1}
Hohlfeld (1996) [6]	6.87×10^{-4}	1.10×10^{-1}	1.97×10^{-1}
Papadogiannis (1997) [7]	4.19×10^{-5}	3.91×10^{-4}	5.85×10^{-3}
Bartoli (1997) [8]	5.94×10^{-4}	1.75×10^{-2}	1.17×10^{-1}
Farztidinov (1999) [9]	3.13×10^{-5}	2.85×10^{-3}	4.11×10^{-2}
	3.52×10^{-4}	6.28×10^{-3}	8.64×10^{-2}
	4.09×10^{-4}	7.43×10^{-2}	1.01×10^{-1}
Bonn (2000) [10]	1.76×10^{-4}	8.47×10^{-3}	1.68×10^{-2}
Kruglyak (2005) [11]	1.34×10^{-3}	1.57×10^{-3}	
Ligges (2009/11) [12 and 13]	1.76×10^{-4}	5.30×10^{-3}	
Shen (2015) [14]	1.41×10^{-3}	1.14×10^{-3}	2.09×10^{-2}
Nakamura (2016) [15]	3.00×10^{-3}	2.82×10^{-2}	
Mo (2018) [16]	1.76×10^{-4}	9.05×10^{-3}	4.21×10^{-2}
Obergfell (2020) [17]	1.41×10^{-3}	1.12×10^{-3}	6.52×10^{-2}
Suemoto (2021) [18]	3.06×10^{-3}	3.23×10^{-3}	1.59×10^{-2}

TABLE S2. Values of β/δ and range of α values (indicated by α_{\min} and α_{\max}) in experimental investigations of room-temperature Ag excited by sub-ps laser pulses. Experiments with only α_{\min} indicated were carried out at a single excitation level.

Ag			
Study	β/δ	α_{\min}	α_{\max}
Riffe (1993) [19]	3.96×10^{-4}	2.82×10^{-3}	1.04×10^{-1}
Groneveld (1995) [20]	3.96×10^{-4}	3.05×10^{-5}	1.31×10^{-4}
Hohlfeld (1996) [6]	4.16×10^{-4}	4.88×10^{-2}	9.29×10^{-2}
Del Fatti (1998) [21]	1.04×10^{-3}	1.46×10^{-5}	1.82×10^{-3}
Del Fatti (2000) [22]	1.04×10^{-3}	1.45×10^{-5}	5.78×10^{-4}
Kruglyak (2005) [11]	8.11×10^{-4}	1.64×10^{-3}	
Owens (2010) [23]	4.57×10^{-4}	4.61×10^{-3}	1.82×10^{-2}
	2.77×10^{-4}	1.77×10^{-2}	
Ligges (2011) [13]	1.06×10^{-4}	2.45×10^{-3}	
Oguz Er (2013) [24]	3.16×10^{-5}	1.02×10^{-2}	1.60×10^{-2}
Suemoto (2021) [18]	1.85×10^{-3}	3.21×10^{-3}	1.59×10^{-2}

TABLE S3. Values of β/δ and range of α values (indicated by α_{\min} and α_{\max}) in experimental investigations of room-temperature Au excited by sub-ps laser pulses. Experiments with only α_{\min} indicated were carried out at a single excitation level.

Au			
Study	β/δ	α_{\min}	α_{\max}
Schoenlein (1987) [25]	4.47×10^{-4}	7.34×10^{-4}	7.29×10^{-3}
Brorson (1987) [26]	4.47×10^{-4}	1.51×10^{-3}	2.94×10^{-3}
Elsayed-Ali (1991) [27]	4.16×10^{-4}	9.72×10^{-4}	1.57×10^{-2}
Fann (1992) [28]	5.47×10^{-4}	4.27×10^{-3}	1.06×10^{-2}
Juhasz (1992) [29]	4.16×10^{-4}	1.38×10^{-4}	
Juhasz (1993) [30]	4.26×10^{-4}	1.24×10^{-4}	2.43×10^{-4}
Girardeau-Montaut (1993) [31]	2.73×10^{-5}	2.22×10^{-4}	8.85×10^{-4}
Sun (1993) [32]	1.79×10^{-3}	4.32×10^{-5}	9.18×10^{-3}
Sun (1994) [33]	1.22×10^{-3}	7.79×10^{-5}	
	2.16×10^{-3}	1.02×10^{-4}	
Wang (1994) [34]	4.47×10^{-4}	1.85×10^{-2}	2.16×10^{-1}
Groneveld (1995) [20]	4.26×10^{-4}	2.73×10^{-5}	1.18×10^{-4}
Hohlfeld (1996) [6]	4.47×10^{-4}	7.89×10^{-2}	1.45×10^{-1}
Hohlfeld (1997) [35]	1.14×10^{-4}	4.75×10^{-3}	1.22×10^{-2}
Maznev (1997) [36]	9.15×10^{-4}	9.84×10^{-2}	
Moore (1999) [37]	9.15×10^{-4}	6.58×10^{-5}	6.28×10^{-3}
Hibara (1999) [38]	1.14×10^{-4}	2.21×10^{-3}	1.29×10^{-2}
Hostetler (1999) [39]	8.81×10^{-4}	5.92×10^{-4}	1.06×10^{-3}
Bonn (2000) [10]	1.14×10^{-4}	1.16×10^{-2}	2.29×10^{-2}
Del Fatti (2000) [22]	1.12×10^{-3}	1.44×10^{-5}	5.78×10^{-4}
Smith (2000) [40]	8.81×10^{-4}	2.01×10^{-3}	4.81×10^{-3}
Smith (2001) [41]	9.15×10^{-4}	2.84×10^{-4}	1.42×10^{-3}
Guo (2001) [42]	9.15×10^{-4}	1.02×10^{-1}	
Ibrahim (2004) [43]	9.15×10^{-4}	1.95×10^{-4}	2.39×10^{-3}
Kruglyak (2005) [11]	8.72×10^{-4}	1.20×10^{-3}	
Hopkins (2007) [44]	9.15×10^{-4}	1.47×10^{-4}	3.88×10^{-3}
Ma (2010) [45]	9.15×10^{-4}	6.67×10^{-5}	2.00×10^{-4}
Hopkins (2011) [46]	8.65×10^{-4}	1.00×10^{-3}	7.83×10^{-3}
Chen (2011) [47]	1.14×10^{-4}	2.66×10^{-2}	1.11×10^{-1}
Ligges (2009/11) [12 and 13]	1.14×10^{-4}	8.56×10^{-3}	
Della Valle (2012) [48]	1.24×10^{-3}	1.53×10^{-3}	
Kolomenskii (2013) [49]	9.15×10^{-4}	1.51×10^{-2}	4.25×10^{-2}
	1.14×10^{-4}	2.06×10^{-2}	
Hopkins (2013) [50]	1.14×10^{-4}	1.47×10^{-3}	1.85×10^{-2}
Guo (2014) [51]	9.15×10^{-4}	1.77×10^{-3}	7.06×10^{-3}
White (2014) [52]	9.15×10^{-4}	3.32×10^{-5}	
Chase (2016) [53]	9.15×10^{-4}	9.15×10^{-3}	
Nakamura (2016) [15]	1.95×10^{-3}	7.41×10^{-3}	2.00×10^{-2}
Sokolowski-Tinten (2017) [54]	1.14×10^{-4}	2.53×10^{-3}	2.64×10^{-2}
Heilpern (2018) [55]	3.09×10^{-3}	1.37×10^{-3}	
Yao (2018) [56]	9.15×10^{-4}	2.76×10^{-3}	1.44×10^{-2}
Sielcken (2020) [57]	4.59×10^{-2}	5.46×10^{-2}	1.12×10^{-1}
Lu (2020) [58]	9.15×10^{-4}	1.09×10^{-1}	
Tomko (2021) [59]	2.51×10^{-4}	2.86×10^{-3}	
Suemoto (2021) [18]	1.99×10^{-3}	3.86×10^{-3}	1.89×10^{-2}
Grauby (2022) [60]	9.15×10^{-4}	1.12×10^{-3}	8.79×10^{-2}

TABLE S4. Values of β/δ and range of α values (indicated by α_{\min} and α_{\max}) in experimental investigations of room-temperature Al excited by sub-ps laser pulses. Experiments with only α_{\min} indicated were carried out at a single excitation level.

Al			
Study	β/δ	α_{\min}	α_{\max}
Riffe (1993) [19]	1.01×10^{-3}	7.54×10^{-3}	1.71×10^{-1}
Tas (1994) [61]	1.07×10^{-3}	3.02×10^{-4}	
Hostetler (1999) [39]	2.08×10^{-3}	8.93×10^{-3}	1.22×10^{-2}
Stevens (2005) [62]	2.08×10^{-3}	9.43×10^{-4}	
Park (2005) [63]	2.08×10^{-3}	2.39×10^{-2}	
Nie (2006) [64]	2.08×10^{-3}	1.36×10^{-2}	
Ma (2013) [65]	2.16×10^{-3}	5.75×10^4	
Waldecker (2016) [66]	2.16×10^{-3}	1.35×10^{-2}	8.27×10^{-2}

SII. ANALYSIS OF NUMERICAL RELAXATION-TIME DATA

In Sec. IV.A.2 of the paper we discuss the fitting of our numerical data for $\tau_H\beta$, $\tau_E\beta$, and $\tau_{th}\beta$ vs β/δ to Eqs. (30), (36) and (40)/(41), respectively. Here we provide details of the fitting procedure. Because normalized relaxation times $\tau\beta$ can vary by several orders of magnitude over the relevant range of β/δ , we utilize $\log(\tau\beta)$ in our analysis. Specifically, our goodness-of-fit function is defined to be

$$\chi^2 = \sum_i [\log(\mathbb{F}(\mathbf{X}, (\beta/\delta)_i) - \log(\tau_i\beta_i)]^2, \quad (\text{S6})$$

where \mathbb{F} is the fitting function and \mathbf{X} represents the set of fitting parameters. In the analysis of $\tau_H\beta$ and $\tau_{th}\beta$ separate fittings are done for each value of γ ($= 0.0086, 0.0172, \text{ and } 0.0344$). In analysis of $\tau_E\beta$ the data obtained at all three values of γ are simultaneously fit, and so in this case $\mathbb{F} = \mathbb{F}(\mathbf{X}, \gamma_i, (\beta/\delta)_i)$.

The numerical data and fits for all three relaxation times are shown in Fig. S1. For $\tau_H\beta$ the value of the fitted exponent a in Eq. (30) is indicated in each panel of Fig. S1. Notice it is quite close to 0.95 for all three cases. For $\tau_{th}\beta$ the exponent b in Eq. (40) depends upon β/δ , as expressed by Eq. (41),

$$b = \frac{b_0 + b_1 \beta/\delta}{1 + b_1 \beta/\delta}.$$

The exponent b for each value of γ is plotted vs β/δ in Fig. 8. Fitted values of b_0 and b_1 are reported in Table S5. For $\tau_E\beta$ the best-fit parameters of Eq. (36) are presented in Table IV.

TABLE S5. Fitted values of b_0 and b_1 in Eq. (41) for three values of γ .

γ	b_0	b_1
0.0086	0.4173	0.4811
0.0172	0.5145	0.5168
0.0344	0.6475	0.7379

We have also fit our data to determine the dependence of $\tau_{th}\delta$ on γ in the $\beta \rightarrow 0$ limit (*ee* scattering only). For this analysis we have also calculated $\tau_{th}\delta$ at three more values of γ : 0.01, 0.02, and 0.0274. These data and a power-law fit are shown in Fig. S2. As the figure shows, $\tau_{th}\delta = 3.33 + 0.059\gamma^{-1.83}$ provides an excellent description of the calculated relaxation times. For comparison Fig. S2 also displays the Gusev and Wright⁶⁷ result, which is given by Eq. (42) as

$$\tau_{th}^G \delta = \left(\frac{2}{\pi}\right)^5 \left[\frac{\ln(2)}{\gamma}\right]^2.$$

This equation yields values that are within a factor of two of our numerical results.

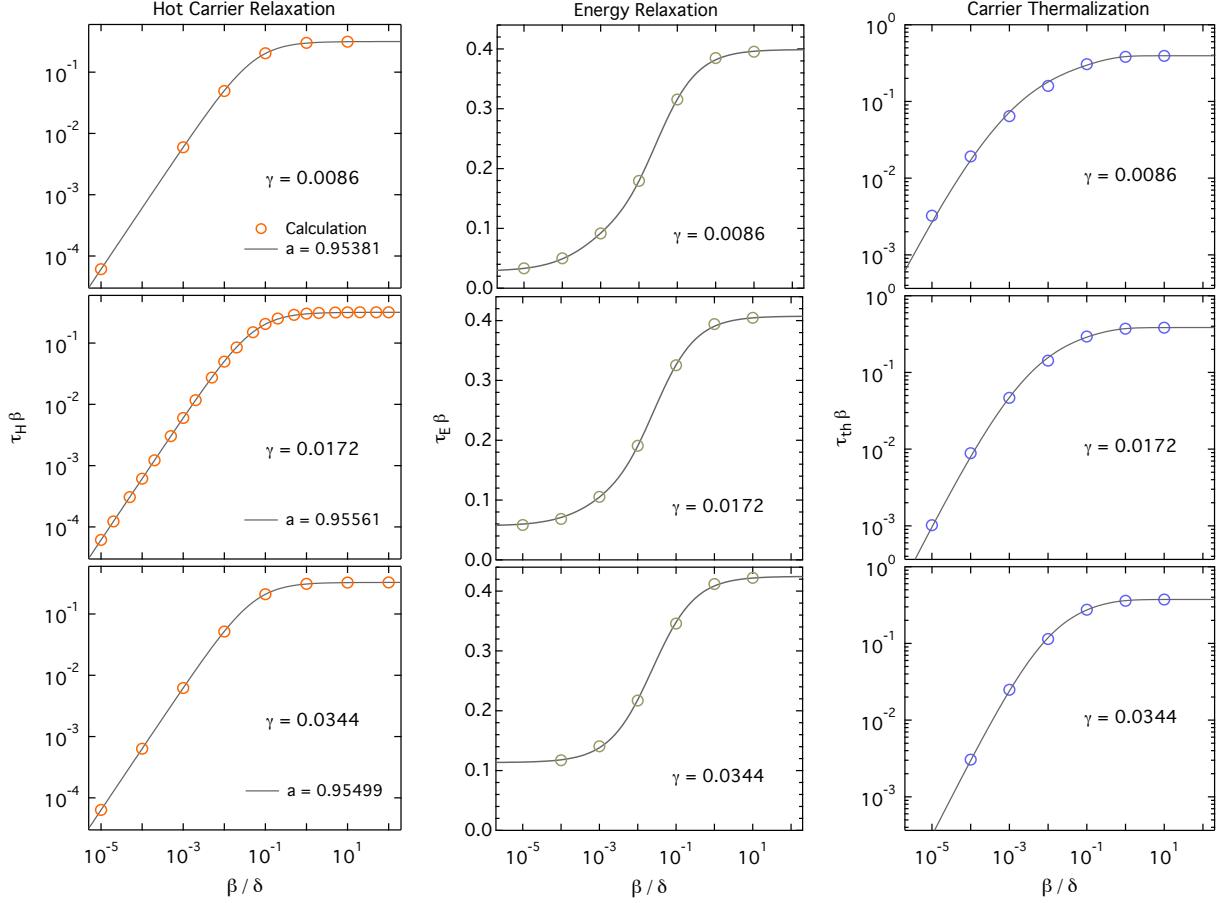


FIG. S1. Numerical relaxation-time data (circles) and least-squares fits (smooth curves) of those data. All relaxations time are normalized by $\beta = K_{ep}/(h\nu)$, the normalized ep interaction strength.

III. INITIAL TIME DEPENDENCE OF $f(\epsilon, t)$

Here we derive an approximate expression for the initial time dependence of the distribution function $f(\epsilon, t)$. As can be ascertained from Figs. 3 and 4 in the paper, the early-time ($t\delta \lesssim 2$) dynamics of the distribution are dominated by electron-electron scattering when $\beta/\delta \leq 10^{-2}$, a range that includes all metals in Table I when excited by photon energies in the near-IR, visible, or uv. For low excitation levels we are thus justified in describing the initial time dependence of the distribution function with an approximate, linearized ee scattering integral derived by Tas and Maris.⁶¹ We note their scattering integral was also obtained assuming a constant density of states and $k_B T_p \ll h\nu$. Using that scattering integral we obtain the integro-differential equation

$$\frac{d\phi(\delta\epsilon, t)}{dt} = -K_{ee} \left[\frac{(\delta\epsilon)^2}{2} \phi(\delta\epsilon, t) - 3 \int_{\delta\epsilon}^{\infty} d(\delta\epsilon') (\delta\epsilon' - \delta\epsilon) \phi(\delta\epsilon', t) \right]. \quad (\text{S7})$$

Recall from the Appendix $\phi(\delta\epsilon, t) = f(\delta\epsilon, t) - f_{FD}(\delta\epsilon, T_p)$. The first term on the right side of Eq. (S7) describes scattering out of states with energy $\delta\epsilon$ [and is consistent with the single-carrier relaxation time given by Eq. (9)], while the second describes electron excitation into these same states. We now set $t = 0$ in Eq. (S7), use the approximate expression for $\phi(\delta\epsilon, 0)$ as given by Eq. (A5), and thence evaluate the integral to find the initial rate of change in $\phi(\delta\epsilon, t)$ is given by

$$\left. \frac{d\phi(\delta\epsilon, t)}{dt} \right|_{t=0} = K_{ee} \alpha \left[(\delta\epsilon)^2 - 3h\nu \delta\epsilon + \frac{3}{2} (h\nu)^2 \right]. \quad (\text{S8})$$

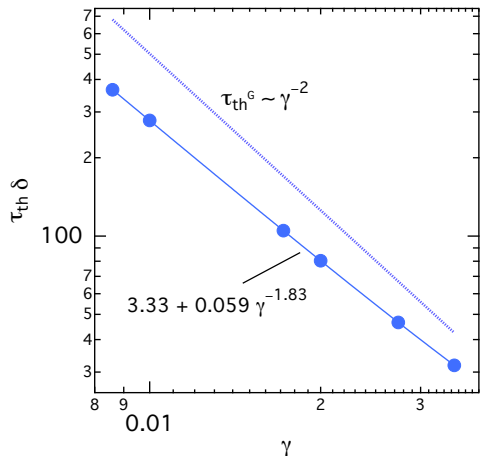


FIG. S2. Numerical values of $\tau_{th}\delta$ vs γ (circles) in the $\beta \rightarrow 0$ limit and least squares fit (solid line) to a power law. The τ_{th}^G result of Gusev and Wright⁶⁷ is also shown (dotted line).

To be clear, this expression is valid for $0 \leq \delta\epsilon \leq h\nu$ [and for $\delta\epsilon > h\nu$ the function $\phi(\delta\epsilon, t)$ is zero]. For small values of $\delta\epsilon$ the quantity in brackets in Eq. (S8) is positive, indicating that initially ϕ initially increases. Conversely, for large values of $\delta\epsilon$ the quantity in brackets is negative, indicating an initial decrease in ϕ . These two behaviors are separated by the energy

$$\delta\epsilon_0 = (3 - \sqrt{3})/2 h\nu = 0.634 h\nu. \quad (\text{S9})$$

As mentioned in Sec. IV.A.1, in part (a) of Fig. 3 and in five panels of Fig. 4 we have marked $\delta\epsilon_0/h\nu$ with a vertical arrow. As can be seen in these figures, for $\delta\epsilon < \delta\epsilon_0$ ($\delta\epsilon > \delta\epsilon_0$) the distribution function indeed initially increases (decreases).

REFERENCES

- ¹D. A. Papaconstantopoulos, *Handbook of the Band Structure of Elemental Solids* (Springer, New York, 1986).
- ²J. R. Reitz, F. J. Milford, and R. W. Christy, *Foundations of Electromagnetic Theory* (Addison-Wesley, 1993).
- ³J. D. Jackson, *Classical Electrodynamics* (John Wiley & Sons, 1975).
- ⁴H. E. Elsayed-Ali, T. B. Norris, M. A. Pessot, and G. A. Mourou, “Time-resolved observation of electron-phonon relaxation in copper,” *Phys. Rev. Lett.* **58**, 1212–1215 (1987).
- ⁵J. Hohlfeld, D. Grosenick, U. Conrad, and E. Matthias, “Femtosecond time-resolved reflection second-harmonic generation on polycrystalline copper,” *Applied Physics A* **60**, 137–142 (1995).
- ⁶J. Hohlfeld, U. Conrad, and E. Matthias, “Does femtosecond time-resolved second-harmonic generation probe electron temperatures at surfaces?” *Applied Physics B* **63**, 541–544 (1996).
- ⁷N. A. Papadogiannis, S. D. Moustazis, and J. P. Girardeau-Montaut, “Electron relaxation phenomena on a copper surface via nonlinear ultrashort single-photon photoelectric emission,” *Journal of Physics D: Applied Physics* **30**, 2389–2396 (1997).
- ⁸A. Bartoli, G. Ferrini, L. Fini, G. Gabetta, F. Parmigiani, and F. T. Arecchi, “Nonlinear photoemission from W and Cu investigated by total-yield correlation measurements,” *Phys. Rev. B* **56**, 1107–1110 (1997).
- ⁹V. Farztdinov, A. Dobryakov, S. Kovalenko, D. Lisin, S. Merkulova, F. Pudonin, and Y. E. Lozovik, “Ultrafast phenomena in copper films,” *Physica Scripta* **60**, 579–583 (1999).
- ¹⁰M. Bonn, D. N. Denzler, S. Funk, M. Wolf, S.-S. Wellershoff, and J. Hohlfeld, “Ultrafast electron dynamics at metal surfaces: Competition between electron-phonon coupling and hot-electron transport,” *Phys. Rev. B* **61**, 1101–1105 (2000).
- ¹¹V. V. Kruglyak, R. J. Hicken, M. Ali, B. J. Hickey, A. T. G. Pym, and B. K. Tanner, “Measurement of hot electron momentum relaxation times in metals by femtosecond ellipsometry,” *Phys. Rev. B* **71**, 233104 (2005).
- ¹²M. Ligges, I. Rajkovic, P. Zhou, O. Posth, C. Hassel, G. Dumpich, and D. von der Linde, “Observation of ultrafast lattice heating using time resolved electron diffraction,” *Applied Physics Letters* **94**, 101910 (2009).
- ¹³M. Ligges, I. Rajković, C. Streubühr, T. Brazda, P. Zhou, O. Posth, C. Hassel, G. Dumpich, and D. v. d. Linde, “Transient (000)-order attenuation effects in ultrafast transmission electron diffraction,” *Journal of Applied Physics* **109**, 065519 (2011).
- ¹⁴X. Shen, Y. P. Timalisina, T.-M. Lu, and M. Yamaguchi, “Experimental study of electron-phonon coupling and electron internal thermalization in epitaxially grown ultrathin copper films,” *Phys. Rev. B* **91**, 045129 (2015).
- ¹⁵A. Nakamura, T. Shimojima, M. Nakano, Y. Iwasa, and K. Ishizaka, “Electron and lattice dynamics of transition metal thin films observed by ultrafast electron diffraction and transient optical measurements,” *Structural Dynamics* **3**, 064501 (2016).
- ¹⁶M. Mo, V. Becker, B. Ofori-Okai, X. Shen, Z. Chen, B. Witte, R. Redmer, R. Li, M. Dunning, S. Weathersby, *et al.*, “Determination of the electron-lattice coupling strength of copper with ultrafast MeV electron diffraction,” *Review of Scientific Instruments* **89**, 10C108 (2018).
- ¹⁷M. Oberghell and J. Demsar, “Tracking the time evolution of the electron distribution function in copper by femtosecond broadband optical spectroscopy,” *Phys. Rev. Lett.* **124**, 037401 (2020).
- ¹⁸T. Suemoto, K. Yamanaka, N. Sugimoto, Y. Kobayashi, T. Otsu, S. Tani, and T. Koyama, “Relaxation dynamics of hot electrons in the transition metals Au, Ag, Cu, Pt, Pd, and Ni studied by ultrafast luminescence spectroscopy,” *Journal of Applied Physics* **130**, 025101 (2021).
- ¹⁹D. M. Riffe, X. Y. Wang, M. C. Downer, D. L. Fisher, T. Tajima, J. L. Erskine, and R. M. More, “Femtosecond thermionic emission from metals in the space-charge-limited regime,” *JOSA B* **10**, 1424–1435 (1993).
- ²⁰R. H. M. Groeneveld, R. Sprik, and A. Lagendijk, “Femtosecond spectroscopy of electron-electron and electron-phonon energy relaxation in Ag and Au,” *Phys. Rev. B* **51**, 11433–11445 (1995).
- ²¹N. Del Fatti, R. Bouffanais, F. Vallée, and C. Flytzanis, “Nonequilibrium electron interactions in metal films,” *Phys. Rev. Lett.* **81**, 922–925 (1998).
- ²²N. Del Fatti, C. Voisin, M. Achermann, S. Tzortzakis, D. Christofilos, and F. Vallée, “Nonequilibrium electron dynamics in noble metals,” *Phys. Rev. B* **61**, 16956–16966 (2000).
- ²³D. T. Owens, C. Fuentes-Hernandez, J. M. Hales, J. W. Perry, and B. Kippelen, “A comprehensive analysis of the contributions to the nonlinear optical properties of thin Ag films,” *Journal of Applied Physics* **107**, 123114 (2010).
- ²⁴A. Oguz Er, J. Chen, J. Tang, and P. M. Rentzepis, “Transient lattice distortion induced by ultrashort heat pulse propagation through thin film metal/metal interface,” *Applied Physics Letters* **102**, 051915 (2013).
- ²⁵R. W. Schoenlein, W. Z. Lin, J. G. Fujimoto, and G. L. Eesley, “Femtosecond studies of nonequilibrium electronic processes in metals,” *Phys. Rev. Lett.* **58**, 1680–1683 (1987).
- ²⁶S. D. Brorson, J. G. Fujimoto, and E. P. Ippen, “Femtosecond electronic heat-transport dynamics in thin gold films,” *Phys. Rev. Lett.* **59**, 1962–1965 (1987).
- ²⁷H. E. Elsayed-Ali, T. Juhasz, G. O. Smith, and W. E. Bron, “Femtosecond thermorefectivity and thermotransmissivity of polycrystalline and single-crystalline gold films,” *Phys. Rev. B* **43**, 4488–4491 (1991).
- ²⁸W. S. Fann, R. Storz, H. W. K. Tom, and J. Bokor, “Electron thermalization in gold,” *Phys. Rev. B* **46**, 13592–13595 (1992).
- ²⁹T. Juhasz, H. E. Elsayed-Ali, X. H. Hu, and W. E. Bron, “Time-resolved thermorefectivity of thin gold films and its dependence on the ambient temperature,” *Phys. Rev. B* **45**, 13819–13822 (1992).
- ³⁰T. Juhasz, H. E. Elsayed-Ali, G. O. Smith, C. Suárez, and W. E. Bron, “Direct measurements of the transport of nonequilibrium electrons in gold films with different crystal structures,” *Phys. Rev. B* **48**, 15488–15491 (1993).
- ³¹J. P. Girardeau-Montaut, C. Girardeau-Montaut, S. D. Moustazis, and C. Fotakis, “High current density produced by femtosecond nonlinear single-photon photoelectric emission from gold,” *Applied Physics Letters* **62**, 426–428 (1993).

- ³²C.-K. Sun, F. Vallée, L. Acioli, E. P. Ippen, and J. G. Fujimoto, “Femtosecond investigation of electron thermalization in gold,” *Phys. Rev. B* **48**, 12365–12368 (1993).
- ³³C.-K. Sun, F. Vallée, L. H. Acioli, E. P. Ippen, and J. G. Fujimoto, “Femtosecond-tunable measurement of electron thermalization in gold,” *Phys. Rev. B* **50**, 15337–15348 (1994).
- ³⁴X. Y. Wang, D. M. Riffe, Y.-S. Lee, and M. C. Downer, “Time-resolved electron-temperature measurement in a highly excited gold target using femtosecond thermionic emission,” *Phys. Rev. B* **50**, 8016–8019 (1994).
- ³⁵J. Hohlfeld, J. G. Müller, S.-S. Wellershoff, and E. Matthias, “Time-resolved thermorefectivity of thin gold films and its dependence on film thickness,” *Applied Physics B* **64**, 387–390 (1997).
- ³⁶A. A. Maznev, J. Hohlfeld, and J. Güdde, “Surface thermal expansion of metal under femtosecond laser irradiation,” *Journal of Applied Physics* **82**, 5082–5085 (1997).
- ³⁷K. L. Moore and T. D. Donnelly, “Probing nonequilibrium electron distributions in gold by use of second-harmonic generation,” *Optics Letters* **24**, 990–992 (1999).
- ³⁸A. H. A. Hibara, T. M. T. Morishita, I. T. I. Tsuyumoto, A. H. A. Harata, T. K. T. Kitamori, and T. S. T. Sawada, “Direct measurements of femtosecond energy dissipation processes of hot electrons in a gold film,” *Japanese Journal of Applied Physics* **38**, 2983 (1999).
- ³⁹J. L. Hostetler, A. N. Smith, D. M. Czajkowsky, and P. M. Norris, “Measurement of the electron-phonon coupling factor dependence on film thickness and grain size in Au, Cr, and Al,” *Appl. Opt.* **38**, 3614–3620 (1999).
- ⁴⁰A. N. Smith, J. L. Hostetler, and P. M. Norris, “Thermal boundary resistance measurements using a transient thermoreflectance technique,” *Microscale Thermophysical Engineering* **4**, 51–60 (2000).
- ⁴¹A. N. Smith and P. M. Norris, “Influence of intraband transitions on the electron thermoreflectance response of metals,” *Applied Physics Letters* **78**, 1240–1242 (2001).
- ⁴²C. Guo, G. Rodriguez, and A. J. Taylor, “Ultrafast dynamics of electron thermalization in gold,” *Phys. Rev. Lett.* **86**, 1638–1641 (2001).
- ⁴³W. M. G. Ibrahim, H. E. Elsayed-Ali, C. E. Bonner, and M. Shinn, “Ultrafast investigation of electron dynamics in multi-layer metals,” *International Journal of Heat and Mass Transfer* **47**, 2261–2268 (2004).
- ⁴⁴P. E. Hopkins and P. M. Norris, “Substrate influence in electron-phonon coupling measurements in thin Au films,” *Applied Surface Science* **253**, 6289–6294 (2007).
- ⁴⁵W. G. Ma, H. D. Wang, X. Zhang, and W. Wang, “Experiment study of the size effects on electron-phonon relaxation and electrical resistivity of polycrystalline thin gold films,” *Journal of Applied Physics* **108**, 064308 (2010).
- ⁴⁶P. E. Hopkins, L. M. Phinney, and J. R. Serrano, “Re-examining electron-Fermi relaxation in gold films with a nonlinear thermoreflectance model,” *Journal of Heat Transfer* **133**, 044505 (2011).
- ⁴⁷J. Chen, W.-K. Chen, and P. M. Rentzepis, “Blast wave and contraction in au (111) thin film induced by femtosecond laser pulses. a time resolved x-ray diffraction study,” *Journal of Applied Physics* **109**, 113522 (2011).
- ⁴⁸G. Della Valle, M. Conforti, S. Longhi, G. Cerullo, and D. Brida, “Real-time optical mapping of the dynamics of nonthermal electrons in thin gold films,” *Phys. Rev. B* **86**, 155139 (2012).
- ⁴⁹A. A. Kolomenskii, R. Mueller, J. Wood, J. Strohaber, and H. A. Schuessler, “Femtosecond electron-lattice thermalization dynamics in a gold film probed by pulsed surface plasmon resonance,” *Applied Optics* **52**, 7352–7359 (2013).
- ⁵⁰P. E. Hopkins, J. C. Duda, B. Kaehr, X. W. Zhou, C.-Y. P. Yang, and R. E. Jones, “Ultrafast and steady-state laser heating effects on electron relaxation and phonon coupling mechanisms in thin gold films,” *Applied Physics Letters* **103**, 211910 (2013).
- ⁵¹L. Guo and X. Xu, “Ultrafast Spectroscopy of Electron-Phonon Coupling in Gold,” *Journal of Heat Transfer* **136**, 122401 (2014).
- ⁵²T. G. White, P. Mabey, D. O. Gericke, N. J. Hartley, H. W. Doyle, D. McGonegle, D. S. Rackstraw, A. Higginbotham, and G. Gregori, “Electron-phonon equilibration in laser-heated gold films,” *Phys. Rev. B* **90**, 014305 (2014).
- ⁵³T. Chase, M. Trigo, A. H. Reid, R. Li, T. Vecchione, X. Shen, S. Weathersby, R. Coffee, N. Hartmann, D. Reis, *et al.*, “Ultrafast electron diffraction from non-equilibrium phonons in femtosecond laser heated Au films,” *Applied Physics Letters* **108**, 041909 (2016).
- ⁵⁴K. Sokolowski-Tinten, X. Shen, Q. Zheng, T. Chase, R. Coffee, M. Jerman, R. Li, M. Ligges, I. Makasyuk, M. Mo, *et al.*, “Electron-lattice energy relaxation in laser-excited thin-film au-insulator heterostructures studied by ultrafast mev electron diffraction,” *Structural Dynamics* **4**, 054501 (2017).
- ⁵⁵T. Heilpern, M. Manjare, A. O. Govorov, G. P. Wiederrecht, S. K. Gray, and H. Harutyunyan, “Determination of hot carrier energy distributions from inversion of ultrafast pump-probe reflectivity measurements,” *Nature Communications* **9**, 1–6 (2018).
- ⁵⁶Q. Yao, L. Guo, V. Iyer, and X. Xu, “Ultrafast electron-phonon coupling at metal-dielectric interface,” *Heat Transfer Engineering* , 1211–1219 (2018).
- ⁵⁷H. J. Sielcken and H. J. Bakker, “Probing the ultrafast electron and lattice dynamics of gold using femtosecond mid-infrared pulses,” *Phys. Rev. B* **102**, 134301 (2020).
- ⁵⁸W. Lu, M. Nicoul, U. Shymanovich, F. Brinks, M. Afshari, A. Tarasevitch, D. Von Der Linde, and K. Sokolowski-Tinten, “Acoustic response of a laser-excited polycrystalline au-film studied by ultrafast Debye-Scherrer diffraction at a table-top short-pulse x-ray source,” *AIP Advances* **10**, 035015 (2020).
- ⁵⁹J. A. Tomko, S. Kumar, R. Sundaraman, and P. E. Hopkins, “Temperature dependent electron-phonon coupling of Au resolved via lattice dynamics measured with sub-picosecond infrared pulses,” *Journal of Applied Physics* **129**, 193104 (2021).
- ⁶⁰S. Grauby, B. Vidal Montes, A. Zenji, J.-M. Rampnoux, and S. Dilhaire, “How to measure hot electron and phonon temperatures with time domain thermoreflectance spectroscopy?” *ACS Photonics* **9**, 3734–3744 (2022).
- ⁶¹G. Tas and H. J. Maris, “Electron diffusion in metals studied by picosecond ultrasonics,” *Phys. Rev. B* **49**, 15046–15054 (1994).

- ⁶²R. J. Stevens, A. N. Smith, and P. M. Norris, “Measurement of thermal boundary conductance of a series of metal-dielectric interfaces by the transient thermoreflectance technique,” *J. Heat Transfer* **127**, 315–322 (2005).
- ⁶³H. Park, X. Wang, S. Nie, R. Clinite, and J. Cao, “Mechanism of coherent acoustic phonon generation under nonequilibrium conditions,” *Phys. Rev. B* **72**, 100301 (2005).
- ⁶⁴S. Nie, X. Wang, H. Park, R. Clinite, and J. Cao, “Measurement of the electronic Grüneisen constant using femtosecond electron diffraction,” *Phys. Rev. Lett.* **96**, 025901 (2006).
- ⁶⁵W. Ma, H. Wang, X. Zhang, and W. Wang, “Study of the electron–phonon relaxation in thin metal films using transient thermoreflectance technique,” *International Journal of Thermophysics* **34**, 2400–2415 (2013).
- ⁶⁶L. Waldecker, R. Bertoni, R. Ernstorfer, and J. Vorberger, “Electron-phonon coupling and energy flow in a simple metal beyond the two-temperature approximation,” *Phys. Rev. X* **6**, 021003 (2016).
- ⁶⁷V. E. Gusev and O. B. Wright, “Ultrafast nonequilibrium dynamics of electrons in metals,” *Phys. Rev. B* **57**, 2878–2888 (1998).